J|A|C|S
ARTICLES
Published on Web 08/01/2002

Hydrocarbon Oxidation by Bis-μ-oxo Manganese Dimers: Electron Transfer, Hydride Transfer, and Hydrogen Atom Transfer Mechanisms

Anna S. Larsen, Kun Wang,[†] Mark A. Lockwood,[‡] Gordon L. Rice,[⊥] Tae-Jin Won,[§] Scott Lovell,[#] Martin Sadílek, František Tureček, and James M. Mayer*

Contribution from the Department of Chemistry, University of Washington, Campus Box 351700, Seattle, Washington 98195-1700

Received February 11, 2002

Abstract: Described here are oxidations of alkylaromatic compounds by dimanganese μ-oxo and μ-hydroxo dimers $[(phen)_2Mn^{IV}(\mu\text{-}O)_2Mn^{IV}(phen)_2]^{4+}$ (**$[Mn_2(O)_2]^{4+}$**), $[(phen)_2Mn^{IV}(\mu\text{-}O)_2Mn^{III}(phen)_2]^{3+}$ (**$[Mn_2(O)_2]^{3+}$**), and $[(phen)_2Mn^{III}(\mu\text{-}O)(\mu\text{-}OH)Mn^{III}(phen)_2]^{3+}$ (**$[Mn_2(O)(OH)]^{3+}$**). Dihydroanthracene, xanthene, and fluorene are oxidized by **$[Mn_2(O)_2]^{3+}$** to give anthracene, bixanthenyl, and bifluorenyl, respectively. The manganese product is the bis(hydroxide) dimer, $[(phen)_2Mn^{III}(\mu\text{-}OH)_2Mn^{II}(phen)_2]^{3+}$ (**$[Mn_2(OH)_2]^{3+}$**). Global analysis of the UV/vis spectral kinetic data shows a consecutive reaction with buildup and decay of **$[Mn_2(O)(OH)]^{3+}$** as an intermediate. The kinetics and products indicate a mechanism of hydrogen atom transfers from the substrates to oxo groups of **$[Mn_2(O)_2]^{3+}$** and **$[Mn_2(O)(OH)]^{3+}$**. **$[Mn_2(O)_2]^{4+}$** is a much stronger oxidant, converting toluene to tolyl-phenylmethanes and naphthalene to binaphthyl. Kinetic and mechanistic data indicate a mechanism of initial preequilibrium electron transfer for *p*-methoxytoluene and naphthalenes because, for instance, the reactions are inhibited by addition of **$[Mn_2(O)_2]^{3+}$**. The oxidation of toluene by **$[Mn_2(O)_2]^{4+}$**, however, is not inhibited by **$[Mn_2(O)_2]^{3+}$**. Oxidation of a mixture of $C_6H_5CH_3$ and $C_6H_5CD_3$ shows a kinetic isotope effect of 4.3 ± 0.8, consistent with C−H bond cleavage in the rate-determining step. The data indicate a mechanism of initial hydride transfer from toluene to **$[Mn_2(O)_2]^{4+}$**. Thus, oxidations by manganese oxo dimers occur by three different mechanisms: hydrogen atom transfer, electron transfer, and hydride transfer. The thermodynamics of e^-, $H^\bullet$, and H^- transfers have been determined from redox potential and pK_a measurements. For a particular oxidant and a particular substrate, the choice of mechanism is influenced both by the thermochemistry and by the intrinsic barriers. Rate constants for hydrogen atom abstraction by **$[Mn_2(O)_2]^{3+}$** and **$[Mn_2(O)(OH)]^{3+}$** are consistent with their 79 and 75 kcal mol^{-1} affinities for $H^\bullet$. In the oxidation of *p*-methoxytoluene by **$[Mn_2(O)_2]^{4+}$**, hydride transfer is thermochemically 24 kcal mol^{-1} more facile than electron transfer; yet the latter mechanism is preferred. Thus, electron transfer has a substantially smaller intrinsic barrier than does hydride transfer in this system.

Introduction

The selective oxidation of hydrocarbons by homogeneous, heterogeneous, and enzymatic agents is of much fundamental and technological interest.[1] The use of hydrocarbons as feedstocks for commodity and fine chemicals typically requires an oxidation step, usually catalyzed by a transition metal compound. Many of the same issues arise in biological and biomimetic oxidations.[2] Progress in these areas will be facilitated by a better mechanistic understanding of how an oxidizing metal site interacts with hydrocarbons. For C−H bond oxidations, there are well-documented reactions that involve initial electron transfer, hydrogen atom transfer, oxidative addition, and electrophilic attack at a C−H bond.[3] Described in this report are oxidations of alkylaromatic compounds by μ-oxo manganese dimers which occur by electron transfer, hydride transfer, or hydrogen atom transfer.[4]

Manganese 1,10-phenanthroline (phen) dimers are a good testing ground for oxidation mechanisms because a number of

* To whom correspondence should be addressed. E-mail: mayer@chem.washington.edu.
[†] Current address: ExxonMobil Research & Engineering Co., Annandale, NJ 08801.
[‡] Current address: Somatocor Pharmaceuticals, Atlanta, GA.
[⊥] Current address: Neah Power Systems Inc., 22118 20th Ave. SE, Suite 142, Bothell, WA 98021.
[§] At UW 1999−2000 on sabbatical leave from Changwon National University, Changwon, South Korea.
[#] Current address: Department of Biochemistry, University of Wisconsin, Madison, WI.

(1) (a) Sheldon, R. A.; Kochi, J. K. *Metal-Catalyzed Oxidation of Organic Compounds*; Academic Press: New York, 1981. (b) Olah, G. A.; Molnár, A. *Hydrocarbon Chemistry*; Wiley: New York, 1995. (c) Special issue on Bioinorganic Enzymology. *Chem. Rev.* **1996**, *96*, 2237−3042. (d) Weissermel, K.; Arpe, H.-J. *Industrial Organic Chemistry*; VCH: New York, 1997.
(2) *Biomimetic Oxidations Catalyzed by Transition Metal Complexes*; Meunier, B., Ed.; Imperial College Press: London, 2000.
(3) (a) Eberson, L. *Electron Transfer Reactions in Organic Chemistry*; Springer-Verlag: Berlin, 1987. (b) Baciocchi, E.; Bietti, Massimo, M.; Lanzalunga, O. *Acc. Chem. Res.* **2000**, *33*, 243−251. (c) Mayer, J. M. *Acc. Chem. Res.* **1998**, *31*, 441−450. (d) Crabtree, R. H. *Chem. Rev.* **1995**, *95*, 987−1007. (e) Shilov, A. E.; Shulpin, G. B. *Chem. Rev.* **1997**, *97*, 2879−2832. (f) Stahl, S. S.; Labinger, J. A.; Bercaw, J. E. *Angew. Chem., Int. Ed.* **1998**, *37*, 2181−2192.

10.1021/ja020204a CCC: $22.00

compounds are available, with different oxidation states and different levels of protonation.[5−8] These and related manganese complexes have long been studied as model systems for the manganese cluster active site of the oxygen evolving complex in Photosystem II.[9−11] There has also been much parallel activity in oxidations by di-μ-oxo complexes of iron, copper, and nickel as models for various metalloenzymes and biomimetic oxidation systems.[12−20]

The development of selective oxidants will be aided by understanding what mechanisms are possible and how each mechanism is affected by the properties of the oxidant and substrate. We argue here that whether reactions occur by electron transfer, hydride transfer, or hydrogen atom transfer depends both on the energetics and on the intrinsic barriers of the various pathways. The separation of driving force and intrinsic barriers is a characteristic of Marcus theory, which was developed for electron transfer reactions.[21] A similar separation has been observed for organic hydrogen atom transfer reactions, where rate constants within a given class correlate with enthalpic driving force (ΔH, from bond strengths) via the Polanyi relation.[22] Studies in our laboratories and elsewhere have found that hydrogen atom abstraction from alkanes and arylalkanes by Cr, Mn, Fe, and Cu complexes can also be understood on the basis of the bond strengths involved.[23,24] Most recently, we have shown that a Marcus-type treatment using self-exchange rates can be successful for hydrogen atom transfer.[25] This follows similar demonstrations for organic hydride transfer reactions by Kreevoy et al.[26] and for proton transfer reactions of metal hydrides by Kristjánsdóttir and Norton.[27] Studies of hydride transfer have been facilitated by Parker's electrochemical determination of hydride affinities,[28] which has been used in understanding reactions of metal hydrides.[29]

Results

I. Synthesis and Characterization of Manganese Dimers. $[(phen)_2Mn^{IV}(\mu\text{-}O)_2Mn^{IV}(phen)_2](ClO_4)_4$ and $[(phen)_2Mn^{IV}(\mu\text{-}O)_2Mn^{III}(phen)_2](PF_6)_3$ (abbreviated $\mathbf{[Mn_2(O)_2]^{4+}}$ and $\mathbf{[Mn_2(O)_2]^{3+}}$) have been previously prepared and structurally characterized.[5−8] The bridging hydroxide dimers $[(phen)_2Mn^{III}(\mu\text{-}O)(\mu\text{-}OH)Mn^{III}(phen)_2](PF_6)_3$ ($\mathbf{[Mn_2(O)(OH)]^{3+}}$) and $[(phen)_2Mn^{III}(\mu\text{-}OH)_2Mn^{II}(phen)_2](PF_6)_3$ ($\mathbf{[Mn_2(OH)_2]^{3+}}$) were each generated from $\mathbf{[Mn_2(O)_2]^{3+}}$and stoichiometric amounts of hydroquinone, following the chemistry of the bipyridine analogue.[30] The compounds were characterized by elemental analysis, IR and optical spectra, mass spectrometry, and cyclic voltammetry. Solution IR spectra of $\mathbf{[Mn_2(O)_2]^{3+}}$ show a band at 686 cm^{-1},[6] which is characteristic of $M_2(\mu\text{-}O)_2$ cores.[31] Exchange with $H_2{}^{18}O$ is rapid (as is typical of $Mn_2(\mu\text{-}O)_2$ compounds[10,11]) and shifts this band to 665 cm^{-1}. Identification of the hydroxide products in reaction mixtures can be problematic because their optical and IR spectra lack distinct bands. Important support for the assignment of these materials was obtained by analysis of their redox state by iodometric titration[32] and/or by addition of hydroquinone and monitoring of its quantitative conversion to benzoquinone by ^1H NMR.

Cyclic voltammetry of $\mathbf{[Mn_2(O)_2]^{3+}}$ in MeCN shows quasi-reversible waves at 0.90 and −0.01 V versus $Cp_2Fe^{+/\circ}$ (Figure 1A), consistent with previous studies.[6,8] These are assigned to the redox couples $\mathbf{[Mn_2(O)_2]^{4+}/[Mn_2(O)_2]^{3+}}$ and $\mathbf{[Mn_2(O)_2]^{3+}/[Mn_2(O)_2]^{2+}}$. $\mathbf{[Mn_2(O)(OH)]^{3+}}$ and $\mathbf{[Mn_2(OH)_2]^{3+}}$ show quasi-reversible reductions at −0.03 and −0.74 V, respectively. Addition of acid to CV solutions causes protonation of the reduced forms, as indicated by the reduction in anodic current (Figure 1B). One equivalent of $[PhNH_3]ClO_4$ ($pK_a = 10.56$[33])

(4) (a) Wang, K.; Mayer, J. M. *J. Am. Chem. Soc.* **1997**, *119*, 1470−1471. (b) Lockwood, M. A.; Wang, K.; Mayer, J. M. *J. Am. Chem. Soc.* **1999**, *121*, 11894−11895.
(5) (a) Goodwin, H. A.; Sylva, R. N. *Aust. J. Chem.* **1965**, *18*, 1743−1749. (b) Goodwin, H. A.; Sylva, R. N. *Aust. J. Chem.* **1967**, *20*, 629−637.
(6) Cooper, S. R.; Calvin, M. *J. Am. Chem. Soc.* **1977**, *99*, 6623−6630.
(7) Manchanda, R.; Brudvig, G. W.; de Gala, S.; Crabtree, R. H. *Inorg. Chem.* **1994**, *33*, 5157−5160.
(8) Stebler, M.; Ludi, A.; Bürgi, H.-B. *Inorg. Chem.* **1986**, *25*, 4743−4750.
(9) (a) Tommos, C.; Babcock, G. T. *Acc. Chem. Res.* **1998**, *31*, 18−25. (b) Wieghardt, K. *Angew. Chem., Int. Ed. Engl.* **1989**, *28*, 1153−1172. (c) Pecoraro, V. L.; Hsieh, W.-Y. In *Metals in Biological Systems*; Sigel, A., Sigel, H., Eds.; Marcel-Dekker: Basel, Switzerland, 2000; Vol. 37, pp 429−504.
(10) Limburg, J.; Vrettos, J. S.; Chen, H.; de Paula, J. C.; Crabtree, R. H.; Brudvig, G. W. *J. Am. Chem. Soc.* **2001**, *123*, 423−430.
(11) Baldwin, M.; Law, N. A.; Stemmler, T. L.; Kampf, J. W.; Penner-Hahn, J. E.; Pecoraro, V. L. *Inorg. Chem.* **1999**, *38*, 4801−4809.
(12) Que, L., Jr. *J. Chem. Soc., Dalton Trans.* **1997**, 3933−3940. (b) Chen, K.; Que, L., Jr. *J. Am. Chem. Soc.* **2001**, *123*, 6327−6337.
(13) Lee, D.; Lippard, S. J. *J. Am. Chem. Soc.* **2001**, *123*, 4611−4612.
(14) Ménage, S.; Galey, J. B.; Dumats, J.; Hussler, G.; Seité, M.; Luneau, I. G.; Chottard, G.; Fontecave, M. *J. Am. Chem. Soc.* **1998**, *120*, 13370−13382.
(15) Tolman, W. B. *Acc. Chem. Res.* **1997**, *30*, 227−237.
(16) Obias, H. V.; Lin, Y.; Murthy, N. N.; Pidcock, E.; Solomon, E. I.; Ralle, M.; Blackburn, N. J.; Neuhold, Y.-M.; Zuberbühler, A. D.; Karlin, K. D. *J. Am. Chem. Soc.* **1998**, *120*, 12960−12961.
(17) Mahadevan, V.; Henson, M. J.; Solomon, E. I.; Stack, T. D. P. *J. Am. Chem. Soc.* **2000**, *122*, 10249−10250.
(18) Elliott, S. J.; Zhu, M.; Tso, L.; Nguyen, H.-H. T.; Yip, J. H.-K.; Chan, S. I. *J. Am. Chem. Soc.* **1997**, *119*, 9949−9955.
(19) Itoh, S.; Bandoh, H.; Nakagawa, M.; Nagatomo, S.; Kitagawa, T.; Karlin, K. D.; Fukuzumi, S. *J. Am. Chem. Soc.* **2001**, *123*, 11168−11178.
(20) Shiren, K.; Ogo, S.; Fujinami, S.; Hayashi, H.; Suzuki, M.; Uehara, A.; Watanabe, Y.; Moro-oka, Y. *J. Am. Chem. Soc.* **2000**, *122*, 254−262.
(21) Marcus, R. A.; Sutin, N. *Biochim. Biophys. Acta* **1985**, *811*, 265. Sutin, N. *Prog. Inorg. Chem.* **1983**, *30*, 441.
(22) (a) Kochi, J. K., Ed. *Free Radicals*; Wiley: New York, 1973; Vol. 1, pp 275−331. (b) Tedder, J. M. *Angew. Chem., Int. Ed. Engl.* **1982**, *21*, 401−410.
(23) (a) Cook, G. K.; Mayer, J. M. *J. Am. Chem. Soc.* **1994**, *116*, 1855−1868 (correction, *J. Am. Chem. Soc.* **1994**, *116*, 8859). (b) Cook, G. K.; Mayer, J. M. *J. Am. Chem. Soc.* **1995**, *117*, 7139−7156. (c) Gardner, K. A.; Mayer, J. M. *Science* **1995**, *269*, 1849−1851. (d) Gardner, K. A.; Kuehnert, L. L.; Mayer, J. M. *Inorg. Chem.* **1997**, *36*, 2069−2078. (e) Roth, J. P.; Mayer, J. M. *Inorg. Chem.* **1999**, *38*, 2760−2761. (f) Lockwood, M. A.; Blubaugh, T. J.; Collier, A. M.; Lovell, S.; Mayer, J. M. *Angew. Chem., Int. Ed.* **1999**, *38*, 225−227. (g) Reference 4a.
(24) (a) Jonas, R. T.; Stack, T. D. P. *J. Am. Chem. Soc.* **1997**, *119*, 8566−8567. Goldsmith, C. R.; Jonas, R. T.; Stack, T. D. P. *J. Am. Chem. Soc.* **2002**, *124*, 83−96. (b) Bakac, A. *J. Am. Chem. Soc.* **2000**, *122*, 1092−1097. (c) Strassner, T.; Houk, K. N. *J. Am. Chem. Soc.* **2000**, *122*, 7821−7822. (d) Reitz, J. B.; Solomon, E. I. *J. Am. Chem. Soc.* **1998**, *120*, 11467−11478.
(25) Roth, J. P.; Yoder, J. C.; Won, T.-J.; Mayer, J. M. *Science* **2001**, *294*, 2524−2526.
(26) (a) Kreevoy, M. M.; Oh, S. *J. Am. Chem. Soc.* **1973**, *95*, 4805. (b) Lee, I.-S. H.; Jeoung, E. H.; Kreevoy, M. M. *J. Am. Chem. Soc.* **2001**, *123*, 7492.
(27) Kristjánsdóttir, S. S.; Norton, J. R. *J. Am. Chem. Soc.* **1991**, *113*, 4366−4367.
(28) (a) Cheng, J.-P.; Handoo, K. L.; Parker, V. D. *J. Am. Chem. Soc.* **1993**, *115*, 2655−2660. (b) Handoo, K. L.; Cheng, J.-P.; Parker, V. D. *J. Am. Chem. Soc.* **1993**, *115*, 5067−5072. (c) Parker uses a conversion from measured potentials versus $Cp_2Fe^{+/\circ}$ to values versus NHE of +0.528 V (refs 28a,b, Parker, V. D., personal communication, 1999), which differs from the value for $Cp_2Fe^{+/\circ}$ in acetonitrile quoted by others (cf., Connelly, N. G.; Geiger, W. E. *Chem. Rev.* **1996**, *96*, 877−910).
(29) (a) Cheng, T. Y.; Brunschwig, B. S.; Bullock, R. M. *J. Am. Chem. Soc.* **1998**, *120*, 13121−13127; **1999**, *121*, 3150−3155. (b) Sarker, N.; Bruno, J. W. *J. Am. Chem. Soc.* **1998**, *120*, 2174−2180. (c) Berning, D. E.; Noll, B. C.; DuBois, D. L. *J. Am. Chem. Soc.* **1998**, *120*, 11432−11447.
(30) Ghosh, M. C.; Reed, J. W.; Bose, R. N.; Gould, E. S. *Inorg. Chem.* **1994**, *33*, 73−78.
(31) Costas, M.; Rohde, J. U.; Stubna, A.; Ho, R. Y. N.; Quaroni, L.; Münck, E.; Que, L., Jr. *J. Am. Chem. Soc.* **2001**, *123*, 12931−12932 and references therein.
(32) (a) Jeffery, G. H.; Bassett, J.; Mendham, J.; Denney, R. C. *Vogel's Textbook of Quantitative Chemical Analysis*, 5th ed.; Wiley: New York, 1989; pp 384−391. (b) Lee, D. G.; Perez-Benito, J. F. *J. Org. Chem.* **1988**, *53*, 5725−5728.
(33) Izutsu, K. *Acid−Base Dissociation Constants in Dipolar Aprotic Solvents*; IUPAC Chemical Data Series No. 35; Blackwell Scientific Publications: Boston, MA, 1990.

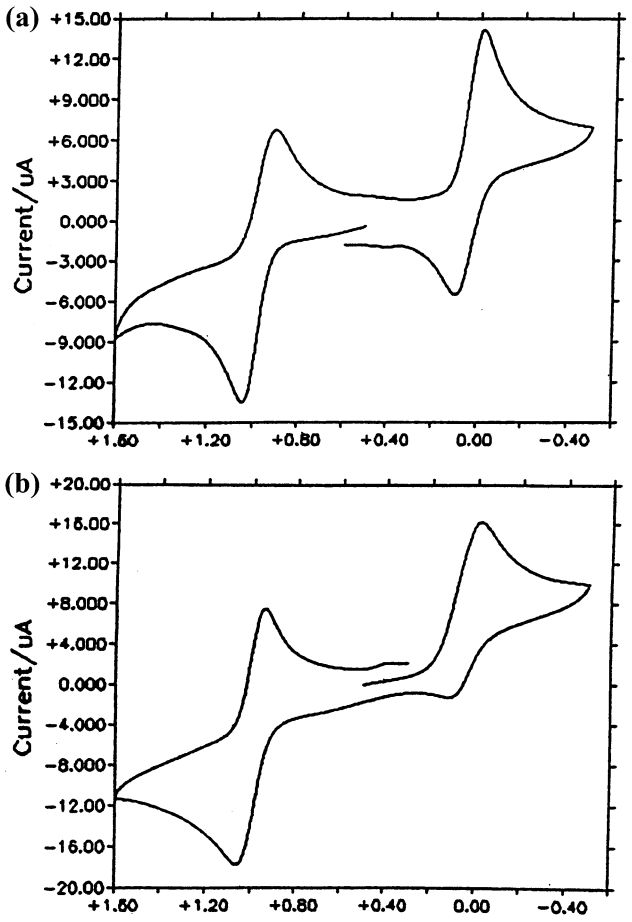

Figure 1. Cyclic voltammograms of 2.5 mM $[Mn_2(O)_2]^{3+}$ in MeCN (100 mV s^{-1}, $^nBu_4NPF_6$, vs $Cp_2Fe^{+/o}$) (A); with added 2.0 mM lutidine H^+ (B).

Scheme 1. Redox Potentials (vs $Cp_2Fe^{+/o}$), pK_a Values, H• and H− Affinities in MeCN

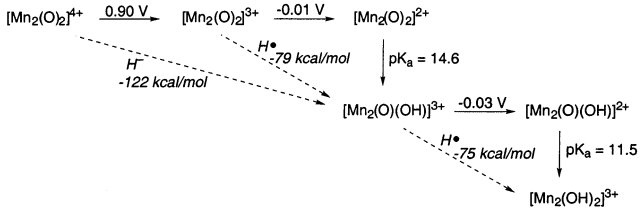

causes complete loss of the anodic current for $[Mn_2(O)_2]^{3+}$, while 1 equiv of NH_4PF_6 (pK_a = 16.46[33]) has no effect. With 2,4-lutidinium perchlorate (pK_a = 14.05[33]), three independent measurements indicated a pK_a of 14.6 ± 0.5 (following the procedure of Baldwin and Pecoraro[34]). Similarly, titrations of solutions of $[Mn_2(O)(OH)]^{3+}$ with $PhNH_3ClO_4$ yielded a pK_a for $[Mn_2(OH)_2]^{3+}$ of 11.5 ± 0.5. The conclusion that the reduced forms are basic is consistent with the reported aqueous electrochemistry.[35] The redox potentials and pK_a values are summarized in Scheme 1 (the values for H• and H^- addition will be discussed below).

All of the dimers are fairly stable in acetonitrile solution (the solvent for all of the reactions reported here). $[Mn_2(O)_2]^{4+}$ solutions, however, decompose rapidly in the presence of excess water or nitrogen bases (pyridine, 2,6-lutidine, 2,6-di-*tert*-butylpyridine, 1,10-phenanthroline), giving predominantly $[Mn_2(O)_2]^{3+}$ (by UV/vis). Comproportionation of $[Mn_2(O)_2]^{4+}$ and $[Mn_2(O)(OH)]^{3+}$ occurs rapidly to form $[Mn_2(O)_2]^{3+}$, although the fate of the proton is uncertain. Adding protons to $[Mn_2(O)_2]^{3+}$ (excess triflic acid) generates $[Mn_2(O)_2]^{4+}$ in ca. 50% yield, apparently by disproportionation. Surprisingly, comproportionation of $[Mn_2(O)_2]^{3+}$and $[Mn_2(OH)_2]^{3+}$ is very slow; the optical spectrum of a mixture of 1 mM solutions of these materials is identical to the sum of the components' spectra. Spectra of the mixture change slowly over 3 days, consistent with partial formation of $[Mn_2(O)(OH)]^{3+}$, but $[Mn_2(O)_2]^{3+}$ is still observed.

II. Oxidations by $[Mn_2(O)_2]^{3+}$: Hydrogen Atom Transfer Reactions. (A) Reaction with 9,10-Dihydroanthracene (DHA). $[Mn_2(O)_2]^{3+}$ reacts with DHA over 12 h at 65 °C in MeCN, with a change in color from olive green to light brown (eq 1).

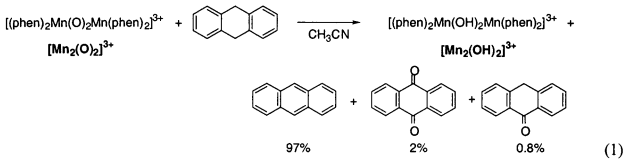

(1)

GC/MS analysis of the products revealed the presence of anthracene and traces of anthrone and anthraquinone. Iodometric titration of the isolated manganese product gave an average oxidation state of 2.37 (±0.04), consistent with the predominant formation of the $Mn^{II}Mn^{III}$ dimer, $[Mn_2(OH)_2]^{3+}$. The observed products account almost quantitatively for the manganese oxidizing equivalents consumed, so eq 1 is close to a balanced reaction. When reaction 1 is run under oxygen, substantially more anthrone and anthraquinone are formed (quantitation is difficult because of the lesser but competing autoxidation of anthracene under these conditions). The influence of O_2 is consistent with the involvement of carbon radicals. Oxidation of a mixture of DHA and DHA-d_{12} (15 μmol each) by $[Mn_2(O)_2]^{3+}$ (15 μmol) at 55 °C gave an anthracene to anthracene-d_{10} ratio of 4.2 ± 0.3 (55 °C) (by GC/MS), indicating a primary isotope effect of ∼4.

The oxidation of excess DHA by $[Mn_2(O)_2]^{3+}$, as monitored by UV/vis spectroscopy, shows no induction period (Figure 2). Absorbance versus time traces indicate a consecutive reaction pattern, with the formation and decay of $[Mn_2(O)(OH)]^{3+}$, because the absorbance at 526 nm increases and then decreases as the reaction proceeds. An isosbestic point at 610 nm is observed in the first phase of reaction, $[Mn_2(O)_2]^{3+} \rightarrow [Mn_2(O)(OH)]^{3+}$, which goes away when the intermediate is converted to $[Mn_2(OH)_2]^{3+}$. The 400−800 nm spectral-kinetic data were processed by SpecFit software[36] utilizing a kinetic model in which both $[Mn_2(O)_2]^{3+}$and $[Mn_2(O)(OH)]^{3+}$ oxidize DHA to the 9-hydroanthracenyl radical (HA•), which is rapidly oxidized to anthracene (A) by both oxidants (Scheme 2). Trapping of HA• (k_{A3}, k_{A4}) is expected to be much faster than reaction with DHA, as the C−H bond strength is substantially weaker in the radical. SpecFit refinements started from ap-

(34) Baldwin, M. J.; Pecoraro, V. L. *J. Am. Chem. Soc.* **1996**, *118*, 11325−11326.

(35) Manchanda, R.; Thorp, H. H.; Brudvig, G. W.; Crabtree, R. H. *Inorg. Chem.* **1992**, *31*, 4040−4041. Attempts in our hands to repeat this aqueous electrochemistry gave evidence (e.g., color changes) that $[Mn_2(O)_2]^{3+}$ was not stable under our conditions.

(36) Binstead, R. A.; Jung, B.; Zuberbühler, A. D. *Specfit/32 Global Analysis System*; Spectrum Software Associates, Malborough, MA; specsoft@compuserve.com.

Table 1. Rate Constants for the Oxidation of Hydrocarbons by $[Mn_2O_2]^{3+}$ in Acetonitrile

substrate (D[C–H][a])	temp, °C	k_1, $M^{-1}s^{-1}$ [b]	k_2, $M^{-1}s^{-1}$ [b]	k_3, $M^{-1}s^{-1}$	k_4, $M^{-1}s^{-1}$
DHA[c] (78)	32	1.2×10^{-3}	3.0×10^{-4}	$\geq 1 \times 10^{5}$ [d]	$\geq 1 \times 10^{4}$ [d]
	40	2.4×10^{-3}	6.7×10^{-4}		
	47	4.3×10^{-3}	1.2×10^{-3}		
	54	7.3×10^{-3}	1.9×10^{-3}		
	64	1.4×10^{-2}	4.4×10^{-3}		
xanthene[e] (76)	20	6.7×10^{-3}	6.4×10^{-3}	2×10^{5} [f]	2×10^{4} [f]
	30	2.2×10^{-2}	1.9×10^{-2}	3×10^{5} [f]	3×10^{4} [f]
	40	3.1×10^{-2}	2.7×10^{-2}	5×10^{5} [f]	5×10^{4} [f]
	50	6.9×10^{-2}	6.7×10^{-2}	6×10^{5} [f]	6×10^{4} [f]
fluorene[e] (80)	55	6.2×10^{-4}	4.3×10^{-4}	2×10^{4} [f]	2×10^{3} [f]
	65	1.3×10^{-3}	1.0×10^{-3}	3×10^{4} [f]	3×10^{3} [f]

[a] Substrate C−H bond dissociation energies, in kcal mol^{-1}, from Table 3. [b] Estimated errors ±20%. [c] Kinetic model in Scheme 2. [d] $k_{A3}/k_{A4} \cong 10$, and $k_{A3} \geq 1 \times 10^5$. [e] Kinetic model in Scheme 3. [f] Estimated errors ±50%.

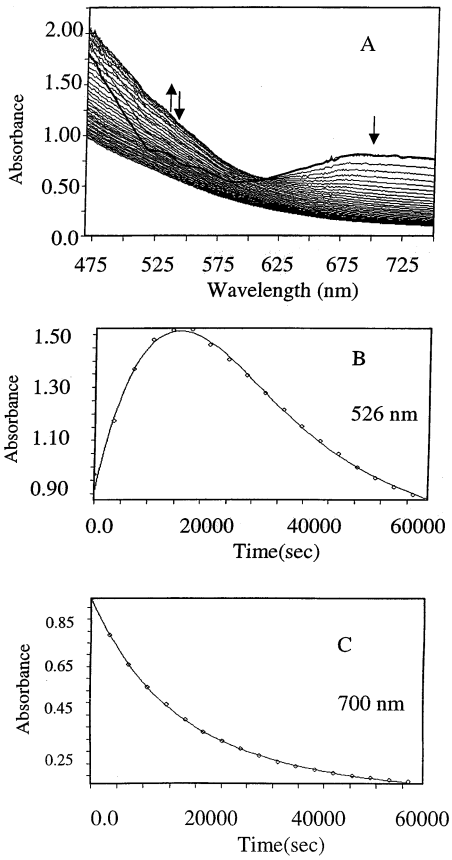

Figure 2. Spectral changes observed for the reaction of $[Mn_2O_2]^{3+}$ and DHA in acetonitrile solution at 32 °C. (A) Overlay of the spectra, with the first spectrum marked by a heavier line. Arrows indicate the sequence and direction of absorbance changes at 526 and 700 nm. (B) and (C): Absorbance changes at 526 and 700 nm, respectively; open circles are experimental data; solid line is from the global kinetic fit (Scheme 2).

Scheme 2. Kinetic Model A, for Oxidation of DHA by $[Mn_2(O)_2]^{3+}$

$$[Mn_2(O)_2]^{3+} + DHA \xrightarrow{k_{A1}} [Mn_2(O)(OH)]_3^{3+} + HA\bullet \quad (A1)$$

$$[Mn_2(O)(OH)]^{3+} + DHA \xrightarrow{k_{A2}} [Mn_2(OH)_2]^{3+} + HA\bullet \quad (A2)$$

$$[Mn_2(O)_2]^{3+} + HA\bullet \xrightarrow{k_{A3}} [Mn_2(O)(OH)]^{3+} + A \quad (A3)$$

$$[Mn_2(O)(OH)]^{3+} + HA\bullet \xrightarrow{k_{A4}} [Mn_2(OH)_2]^{3+} + A \quad (A4)$$

proximate values of $2k_{A1}$ and $2k_{A2}$ that were obtained from pseudo-first-order absorbance/time plots at 700 and 526 nm (the factor of 2 is needed to account for the rapid trapping of HA•). Initial spectra were used to obtain k_{A1}, while k_{A2} was derived from spectral changes after the loss of the isosbestic point.

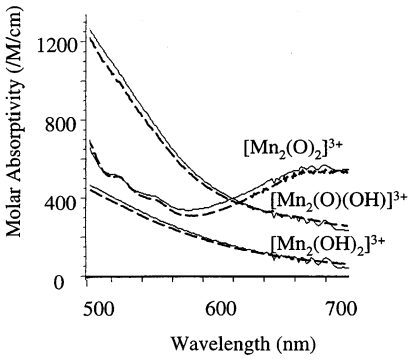

Figure 3. Visible spectra of $[Mn_2(O)_2]^{3+}$, $[Mn_2(O)(OH)]^{3+}$, and $[Mn_2(OH)_2]^{3+}$ measured on independent samples (broken lines) and determined from the global kinetic fit of the data in Figure 2 according to Scheme 2 (solid lines).

Simultaneous refinement of the four rate constants by SpecFit was unsuccessful, so k_{A3} and k_{A4} were entered as fixed parameters and varied manually. Good fits could only be obtained with $k_{A3} \cong 10k_{A4}$ and when both were $>10^4$ M^{-1} s^{-1}. The k_{A3}/k_{A4} ratio in large part determines how much $[Mn_2(O)(OH)]^{3+}$ builds up as an intermediate. The globally optimized fits give the rate constants shown in Table 1.

Various checks provide good support for the kinetic model in Scheme 2. Figure 2 shows the close agreement between experimental and modeled absorbance versus time changes. The spectra predicted for the colored species by the global fit closely match the observed spectra for $[Mn_2(O)_2]^{3+}$, $[Mn_2(O)(OH)]^{3+}$, and $[Mn_2(OH)_2]^{3+}$ (Figure 3). Independent experiments showed that $[Mn_2(O)(OH)]^{3+}$ oxidizes DHA to yield anthracene and trace amounts of anthraquinone and anthrone, and the rate constant at 50 °C was in good agreement with the kinetic simulation result for k_{A2}.

Rate constants determined over the temperature range of 32−64 °C (Table 1) give the activation parameters $\Delta H_{A1}^{\ddagger} = 15.2$ (10) kcal mol^{-1}, $\Delta S_{A1}^{\ddagger} = -22$ (3) eu; $\Delta H_{A2}^{\ddagger} = 16.2$ (10) kcal mol^{-1}, $\Delta S_{A2}^{\ddagger} = -22$ (3) eu. The negative entropies of activation are consistent with bimolecular rate-limiting steps and are similar to what we have observed in other hydrogen atom transfer processes.[3c,23] The rate constants reported here are somewhat different from those given in our preliminary report,[4a] in part because of more sophisticated kinetic modeling and in part because the reactions proceed more slowly with more purified materials.

To address whether the cleavage of the dimers occurs during DHA oxidation, a ligand scrambling experiment was carried

Scheme 3. Kinetic Model B, for Oxidation of Xanthene (XnH) by $[Mn_2(O)_2]^{3+}$

$$[Mn_2(O)_2]^{3+} + XnH \xrightarrow{k_{B1}} [Mn_2(O)(OH)]^{3+} + Xn\bullet \quad (B1)$$

$$[Mn_2(O)(OH)]^{3+} + XnH \xrightarrow{k_{B2}} [Mn_2(OH)_2]^{3+} + Xn\bullet \quad (B2)$$

$$[Mn_2(O)_2]^{3+} + Xn\bullet \xrightarrow{k_{B3}} [Mn_2(O)(OH)]^{3+} + Xn{=}O \quad (B3)$$

$$[Mn_2(O)(OH)]^{3+} + Xn\bullet \xrightarrow{k_{B4}} [Mn_2(OH)_2]^{3+} + Xn{=}O \quad (B4)$$

$$2\,Xn\bullet \xrightarrow{k_{B5}} Xn_2 \quad (B5)$$

out. A 1:1 mixture of $[Mn_2(O)_2]^{3+}$ and an analogue with 4,7-dimethylphenanthroline (Me_2phen) ligands was reacted with DHA. (The Me_2phen analogue oxidizes DHA at a rate comparable to that of the phen complex.) After a little more than 1 half-life, analysis of the manganese complexes present by FAB-MS showed $(phen)_4$ and $(Me_2phen)_4$ complexes with only a very small amount of mixed-ligand dimers. A mixture of dimers $[Mn_2(O)_2(phen)_x(Me_2phen)_{(4-x)}]^{3+}$ was independently synthesized from a mixture of phen and Me_2phen and would have been observable by FAB-MS. Thus, the dimers remain intact through the reaction.

(B) Reactions with Fluorene and Xanthene. Fluorene (10 mM) is oxidized by $[Mn_2(O)_2]^{3+}$ (1 mM) at 50 °C to a roughly equal mixture of fluorenone (Fl═O, 0.28 mM) and 9,9-bifluorenyl (Fl_2, 0.20 mM). Xanthene is similarly oxidized by a roughly 10:1 mixture of xanthone (Xn═O) and 9,9′-bixanthenyl (Xn_2). Xn_2 and Fl_2 are most likely formed by coupling of their respective radicals. The presence of fluorenyl radicals is further supported by reaction in the presence of the radical trap $CBrCl_3$, which yields 9-bromofluorene (6%), fluorenone (45%), and traces of bifluorenyl and 9-trichloromethylfluorene (~0.5% each).

Xanthene oxidation is about an order of magnitude faster than that of DHA; fluorene is about an order of magnitude slower (Table 1). Global fitting of the UV/vis spectral data with SpecFit used the kinetic model in Scheme 3. While similar to the scheme used for DHA reactions, in this case, radical trapping by $[Mn_2(O)_2]^{3+}$ and $[Mn_2(O)(OH)]^{3+}$ (k_{B3}, k_{B4}, see below) is assumed to lead to ketone products because neither Xn• nor Fl• has an abstractable hydrogen. The partitioning between ketone and dimer products is due to competition between trapping by manganese and radical coupling (k_{B5}), which occurs at 10^9 M^{-1} s^{-1}.[37] k_{B1} was determined by global analysis of just the first phase of the reaction (which had to be monitored on a stopped-flow instrument for xanthene). With these values fixed, the spectral changes were analyzed by SpecFit over the whole reaction varying only k_{B2} (Figure 4) to give the values in Table 1. Over the range of 20−50 °C, the activation parameters for xanthene are $\Delta H_{B1}^{\ddagger} = 13.3$ (1) kcal mol^{-1}, $\Delta S_{B1}^{\ddagger} = -23$ (3) eu; $\Delta H_{B2}^{\ddagger} = 13.4$ (1) kcal mol^{-1}, $\Delta S_{B2}^{\ddagger} = -23$ (3) eu.

Equations B3 and B4 encompass multiple reaction steps and likely involve multiple manganese compounds and trace water. They are written in this nonbalanced form because no more information is available. It is possible that other manganese products may be formed in addition to the dimers shown, although introduction of additional species in the kinetic model does not improve the overall fit and results in meaningless predicted spectra. k_{B3} and k_{B4} were varied both to give good fits to the spectral data and to match the observed final ratios of Xn═O to Xn_2 (or Fl═O to Fl_2) determined by GC-MS analysis. As found for the DHA reaction, the buildup of $[Mn_2(O)(OH)]^{3+}$ requires $k_{B3} \cong 10k_{B4}$; their magnitude is set by competition with radical coupling (k_{B5}). k_{B3} for xanthene varies from 2×10^5 to 6×10^5 M^{-1} s^{-1} in the 20−50 °C temperature range (Table 1). The concentration profiles from the kinetic fit are shown in Figure 5; it can be seen that xanthone is predominantly produced in the early stages of reaction when the concentrations of $[Mn_2(O)_2]^{3+}$ and $[Mn_2(O)(OH)]^{3+}$ are high. The uncertainties for k_{B3} and k_{B4} are estimated to be ±50%, because the fitting procedure is not very sensitive to their changes, and the product ratios are uncertain by ~15%.

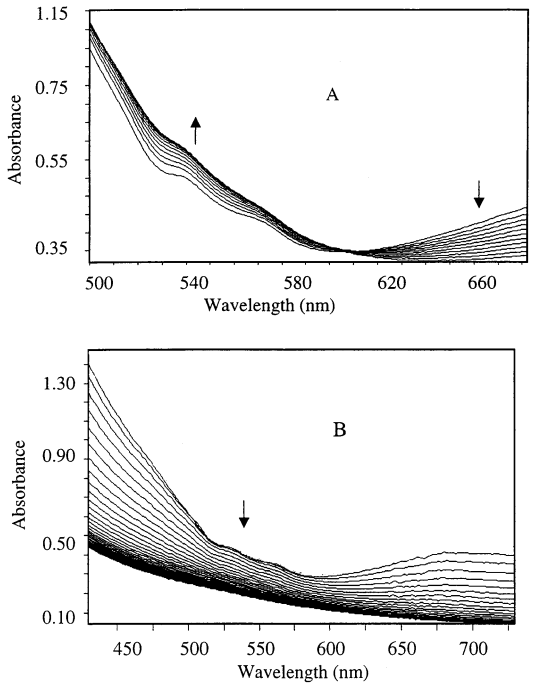

Figure 4. Spectral changes observed for the reaction of $[Mn_2(O)_2]^{3+}$ and xanthene in acetonitrile solution at 40 °C (in both cases, only a few traces are shown for clarity). (A) Spectra obtained by stopped-flow over the first 600 s of a reaction of 1.0 mM $[Mn_2(O)_2]^{3+}$ and 13 mM xanthene (first trace at 10 s; every 60th spectrum shown). (B) Spectra obtained using a diode array spectrophotometer over 7000 s of a reaction of 1.0 mM $[Mn_2(O)_2]^{3+}$ and 12 mM xanthene (first trace at 10 m, spectra taken every 2 min, only a few spectra shown).

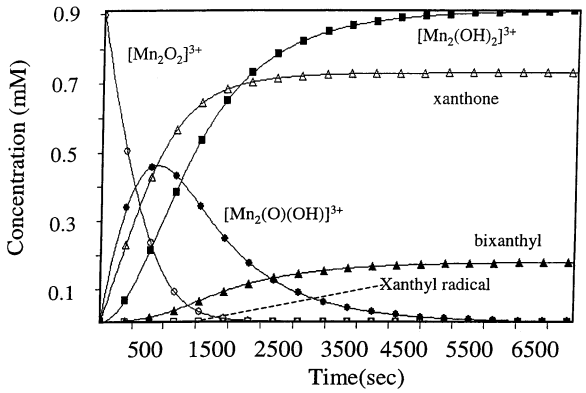

Figure 5. Concentration profiles of all species for the reaction between $[Mn_2(O)_2]^{3+}$ and xanthene derived from global kinetic analysis of the data in Figure 4 (according to Scheme 3). [○, $[Mn_2(O)_2]^{3+}$; ●, $[Mn_2(O)(OH)]^{3+}$; ■, $[Mn_2(OH)_2]^{3+}$; □, xanthyl radical; △, xanthone; ▲, bixanthyl.]

(37) Arends, I. W. C. E.; Mulder, P.; Clark, K. B.; Wayner, D. D. M. *J. Phys. Chem.* **1995**, *99*, 8182−8189.

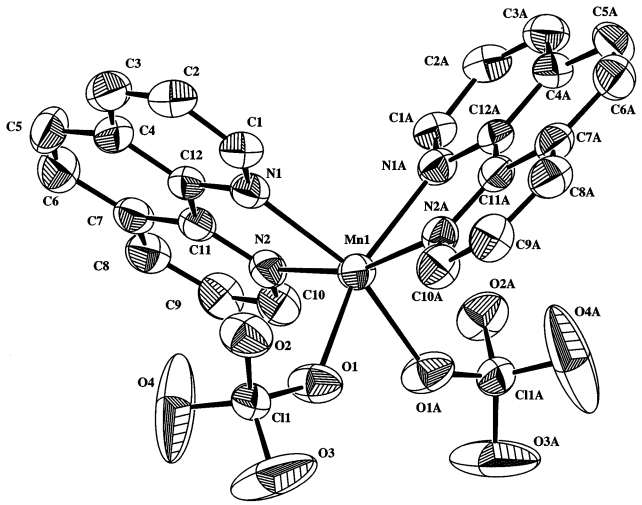

Figure 6. Molecular structure of $Mn(\eta^1\text{-}OClO_3)_2(phen)_2$.

A confirmation of this kinetic model is its ability to predict the changes of the Xn═O to Xn_2 ratio depending on the initial conditions. Increasing the initial xanthene concentration 4 times is predicted to decrease Xn═O/Xn_2 by a factor of 2.6, in reasonable agreement with the observed ratio of 3.8. Quadrupling the initial concentration of $\mathbf{[Mn_2(O)_2]^{3+}}$ was predicted to increase Xn═O/Xn_2 2.1 times, the same as the experimental value. As a further check on the model, the predicted molar absorptivities of the absorbing species are close to the experimentally determined spectra.

Addition of water to the oxidation of fluorene shifts the product ratio substantially toward fluorenone over bifluorenyl (≥10:1). Addition of water at the end of the reaction had no effect. In the presence of excess 20% enriched $H_2{}^{18}O$, the isolated fluorenone is 25 ± 5% enriched, consistent with the rapid exchange of the oxo ligands with $H_2{}^{18}O$ mentioned above.

II. Oxidations by $\mathbf{[Mn_2(O)_2]^{4+}}$: Electron Transfer and Hydride Transfer Reactions. DHA is oxidized by $\mathbf{[Mn_2(O)_2]^{4+}}$ over hours at ambient temperatures to give anthracene, anthrone, and anthraquinone (eq 2). Faster oxidation of DHA by $\mathbf{[Mn_2(O)_2]^{4+}}$ is consistent with it being a more powerful oxidant than $\mathbf{[Mn_2(O)_2]^{3+}}$ ($E_{1/2}$ = +0.90 vs −0.01 V vs $Cp_2Fe^{+/o}$ in MeCN).

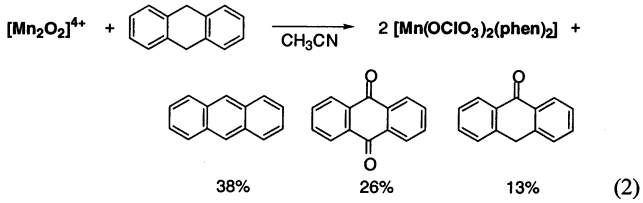

(2)

The average oxidation of the final manganese product in eq 2 was 2.0 (± 0.05), and the organic products account for 85% of manganese oxidative equivalents consumed. Layering the reaction solution with ether precipitates a manganese(II) product, $Mn(OClO_3)_2(phen)_2$. Its X-ray structure shows monomeric pseudo-octahedral molecules, with each perchlorate ion bound η^1 to Mn (Tables S1 and S2; Figure 6). The structure is similar to that of $[Mn(H_2O)_2(phen)_2]^{2+}$ with somewhat longer Mn−O bond lengths, as expected for perchlorate versus water.[38]

Toluene is oxidized by $\mathbf{[Mn_2(O)_2]^{4+}}$ in acetonitrile over 12 h at 65 °C, yielding primarily tolyl-phenylmethane products (*o*:*m*:*p* = 42:7:40 by GC/MS; eq 3). These products, whose identities were confirmed by independent synthesis,[39] are often formed when benzyl cation ($PhCH_2{}^+$) is an intermediate and it

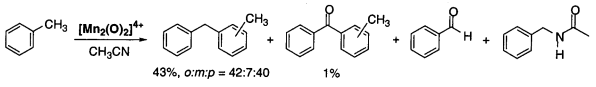

(3)

alkylates the excess toluene present.[40] No bibenzyl was observed, but small amounts of methyl-benzophenones, benzaldehyde, and *N*-benzylacetamide are formed. The yields of benzaldehyde and *N*-benzylacetamide are larger when undried, HPLC grade MeCN is used. Independent oxidation of diphenylmethane by $\mathbf{[Mn_2(O)_2]^{4+}}$ gave exclusively benzophenone; competitive oxidation of toluene and diphenylmethane indicates the latter to be ∼180 times more reactive per benzylic hydrogen. Spectrophotometric titration of the final manganese containing product gave an average oxidation state of 3.52 (± 0.05),[32b] consistent with predominant formation of $\mathbf{[Mn_2(O)_2]^{3+}}$, which is also indicated by the UV/vis spectra of completed reactions. The observed products in the toluene oxidation account for ∼90% of the manganese oxidizing equivalents consumed.

Oxidation of an equimolar mixture of $C_6H_5CH_3$ and $C_6H_5CD_3$ gives d^0, d^2, d^3, and d^5 isotopomers of each of the three isomeric tolyl-phenylmethane products. The d^2 products, for instance, result from attack of $C_6H_5CD_2{}^+$ on $C_6H_5CH_3$. The ratios of products indicate a kinetic isotope effect of 4.3 ± 0.8 on the formation of benzyl cation, consistent with C−H bond cleavage in the rate-determining step. (The apparent isotope effects vary among the isomers and with reaction conditions, consistent with previous studies of related reactions.[41])

p-Xylene is oxidized by $\mathbf{[Mn_2(O)_2]^{4+}}$ to give 2,4′,5-trimethyldiphenylmethane as the primary organic product (by GC-MS, ^{1}H and ^{13}C NMR; eq 4), as expected for an attack of the benzylic cation on the hydrocarbon. As in most of the oxidations of

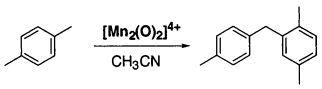

(4)

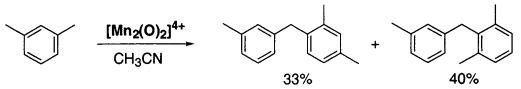

(5)

methylbenzenes by $\mathbf{[Mn_2(O)_2]^{4+}}$, small amounts of analogously substituted benzophenone and acetamide products are also typically observed. *m*-Xylene reacts similarly (eq 5). As a

(38) (a) McCann, M.; Casey, M. T.; Devereux, M.; Curran, M.; McKee, V. *Polyhedron* **1997**, *16*, 2741−2748. (b) Geraghty, M.; McCann, M.; Casey, M. T.; Curran, M.; Devereux, M.; McKee, V.; McCrea, J. *Inorg. Chim. Acta* **1998**, *277*, 257−262.

(39) Friedel−Crafts addition of benzyl chloride to toluene: Hayashi, E.; Takahashi, Y.; Itoh, H.; Yoneda, N. *Bull. Chem. Soc. Jpn.* **1993**, *66*, 3520−3521.

(40) (a) Uemura, S.; Ikeda, T.; Tanaka, S.; Okano, M. *J. Chem. Soc., Perkin Trans. 1* **1978**, 2574−2576. (b) Darbeau, R. W.; White, E. H.; Song, F.; Darbeau, N. R.; Chou, J. *J. Org. Chem.* **1999**, *64*, 5966−5978. (c) Andrulis, P. J., Jr.; Dewar, M. J. S.; Dietz, R.; Hunt, R. L. *J. Am. Chem. Soc.* **1966**, *88*, 5473−5478. (d) Uemura, S.; Tanaka, S.; Okano, M. *J. Chem. Soc., Perkin Trans. 1* **1976**, 1966−1969. (e) Uemura, S.; Ikeda, T.; Tanaka, S.; Okano, M. *J. Chem. Soc., Perkin Trans. 1* **1979**, 2574−2576. (f) McKillop, A.; Turrell, A. G.; Young, D. W.; Taylor, E. C. *J. Am. Chem. Soc.* **1980**, *102*, 6504−6512. (g) Necsoiu, I.; Ghenciulescu, A.; Rentea, M.; Rentea, C. N.; Nenitzescu, C. D. *Rev. Roum. Chim.* **1967**, *12*, 1503−1510. (h) King, S. T. *J. Catal.* **1991**, *131*, 215−225. (i) Bryant, J. R.; Taves, J. E.; Mayer, J. M. *Inorg. Chem.* **2002**, *41*, 2769−2776. (j) Reference 4b.

(41) Effenberger, F.; Maier, A. H. *J. Am. Chem. Soc.* **2001**, *123*, 3429−3433 and references therein.

Table 2. Rate Constants for the Oxidation of Hydrocarbons by $[Mn_2O_2]^{4+}$ in Acetonitrile

substrate	k (M^{-1} s^{-1})[a]	substrate	k (M^{-1} s^{-1})[a]	IE (eV)[b]
$C_6H_5CH_3$[c]	2.9×10^{-5}	naphthalene	4.6	8.14
m-$C_6H_4(CH_3)_2$[d]	2.9×10^{-4}	2-methylnaphthalene	5.1×10^{2}	7.96(3)
p-$C_6H_4(CH_3)_2$[e]	2×10^{-3}	1-methylnaphthalene	6.2×10^{2}	7.91(6)
p-$MeOC_6H_4CH_3$	1.1×10^{2}	2,6-dimethylnaphthalene	1.8×10^{3}	7.78(10)
p-$MeOC_6H_4CH_3$ + $[Mn_2O_2]^{3+}$[f]	1.0×10^{1}	2,6-dimethylnaphthalene + $[Mn_2O_2]^{3+}$[g]	3.4×10^{2}	

[a] Rate constants ($\pm \leq 20\%$) for the reaction of $[Mn_2O_2]^{4+}$ with the given substrate at 298 K in MeCN. Experimental details are given in the Experimental Section; products are given in the text. For the first three entries, these are calculated from $\Delta H^{\ddagger}$ and $\Delta S^{\ddagger}$ measured at higher temperatures. [b] Ionization energies in eV.[50] [c] From rate constants measured at 308−358 K: $\Delta H^{\ddagger} = 16.8 \pm 1.0$ kcal mol^{-1} and $\Delta S^{\ddagger} = -23 \pm 3$ cal K^{-1} mol^{-1}. [d] From rate constants measured at 298−328 K: $\Delta H^{\ddagger} = 20 \pm 2$ kcal mol^{-1} and $\Delta S^{\ddagger} = -6 \pm 4$ cal K^{-1} mol^{-1}. [e] From rate constants measured at 308−338 K: $\Delta H^{\ddagger} = 16 \pm 2$ kcal mol^{-1} and $\Delta S^{\ddagger} = -15 \pm 4$ cal K^{-1} mol^{-1}. [f] With added $[Mn_2O_2]^{3+}$ (3.7×10^{-4} M; initial $[Mn_2O_2]^{4+}$ 8.0×10^{-5} M). [g] With added $[Mn_2O_2]^{3+}$ (2.3×10^{-4} M; initial $[Mn_2O_2]^{4+}$ 9.5×10^{-5} M).

mechanistic probe, the oxidation of isodurene (1,2,3,5-tetramethylbenzene) was explored; commercial material containing some durene (1,2,4,5-$C_6H_2Me_4$) was used, and recrystallization does not significantly change the purity. Two predominant products formed (eq 6), along with a number of other materials in trace quantities. The major products result from attack of the 2,4,6-trimethylbenzyl cation on durene and isodurene, as confirmed by observing the same products from Friedel−Crafts alkylation of the isodurene/durene mixture by $ZnCl_2$/2,4,6-trimethylbenzyl chloride.[39]

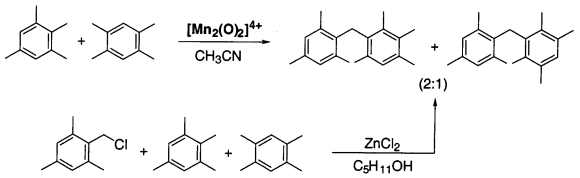

(6)

para-Methoxytoluene reacts much more quickly with $[Mn_2(O)_2]^{4+}$ than do the alkyl-substituted toluenes, while *p*-nitrotoluene is inert to oxidation. *para*-Methoxytoluene gives primarily biaryl species, with only ∼2% of the substituted diarylmethanes (eq 7). Oxidation of $CD_3C_6H_4OMe$ gives only the biaryl products, indicating that there is a larger isotope effect (k_H/k_D) for formation of the diarylmethanes.

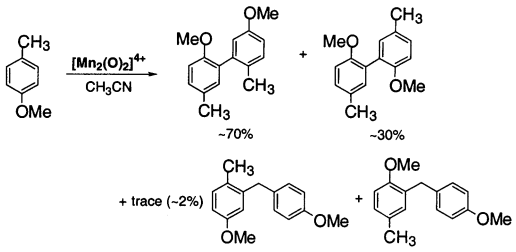

(7)

Naphthalene is oxidized by $[Mn_2(O)_2]^{4+}$ to give binaphthyl as the only identifiable organic product (GC-MS, NMR). The average oxidation state of the isolated manganese product was 3.54 ($\pm$ 0.05), consistent with the formation of the $[Mn_2(O)_2]^{3+}$. The yield of binaphthyl is essentially quantitative. 1-Methyl-, 2-methyl-, and 2,6-dimethyl-naphthalene are oxidized faster than naphthalene, and GC/MS analysis shows formation of binaphthyl products and (in the case of the 2-methyl derivative) some naphthalene carboxaldehyde.

The kinetics of $[Mn_2(O)_2]^{4+}$ oxidations were studied under pseudo-first-order conditions. The toluene and xylene reactions are slow enough to be studied with a diode-array spectrophotometer, but the *p*-methoxytoluene and naphthalene reactions occur on the stopped-flow time scale. Spectral overlays show an isosbestic point at 668 nm and are consistent with a simple $[Mn_2(O)_2]^{4+} \rightarrow [Mn_2(O)_2]^{3+}$ reaction pattern. Both single wavelength and global analyses of the spectra showed first-order kinetics to approximately 3 half-lives. After this time, significant retardation of the reaction rate is often observed, apparently due to the buildup of the reduced species, $[Mn_2(O)_2]^{3+}$. Addition of 4.6 equiv of $[Mn_2(O)_2]^{3+}$ to an independent oxidation of *p*-methoxytoluene by $[Mn_2(O)_2]^{4+}$ led to a reduction in rate of about an order of magnitude. Similarly, addition of 2.4 equiv $[Mn_2(O)_2]^{3+}$ to an oxidation of 2,6-dimethylnaphthalene slowed the rate by roughly a factor of 5. The pseudo-first-order rate constants varied linearly with substrate concentration with a zero intercept within the estimated errors, except for toluene where decomposition of $[Mn_2(O)_2]^{4+}$ was slightly competitive under some conditions (<10%). Selected second-order rate constants and activation parameters are given in Table 2.

Discussion

I. Overview of the Reactions. The oxo-bridged manganese dimers are versatile, multielectron oxidants capable of oxidizing alkylaromatic compounds via different pathways to different products. Because of the basicity of the reduced forms, these reagents often accept both electrons and protons. Mechanisms of alkylarene oxidations have received much attention,[1−3,40,42] and the pathways relevant to the chemistry described here are illustrated in Scheme 4, using toluene as an example. Initial electron transfer forms an arene radical cation, in what is typically an uphill preequilibrium step. Arene radical cations form biaryls (as observed here for naphthalenes and *p*-methoxytoluene) or can be deprotonated to benzylic radicals. Radicals can also be formed directly from the arene by hydrogen atom removal. Radicals can couple (as observed here for xanthene and fluorene), can lose another hydrogen (as in the conversion of DHA to anthracene), or can be oxidized to carbocations. Benzylic carbocations can also be formed by direct removal of a hydride ion. Under the nonnucleophilic conditions used here, the benzylic cation predominantly attacks the excess arene present in a Friedel−Crafts alkylation, forming diarylmethane products.

II. Rate-Limiting Steps. (A) Hydrogen Atom Abstraction by $[Mn_2(O)_2]^{3+}$. A wide range of evidence points to the

(42) (a) Eberson, L. *J. Am. Chem. Soc.* **1983**, *105*, 3192−3199. (b) Reference 40c. (c) Baciocchi, E.; Rol, C.; Mandolini, L. *J. Am. Chem. Soc.* **1980**, *102*, 7597−7598. (d) Baciocchi, E.; D'Acunzo, F.; Galli, C.; Lanzalunga, O. *J. Chem. Soc., Perkin Trans. 2* **1996**, 133−140. (e) Reed, R. A.; Murray, R. W. *J. Phys. Chem.* **1986**, *90*, 3829−3835. (f) Schlesener, C. J.; Amatore, C.; Kochi, J. K. *J. Phys. Chem.* **1986**, *90*, 3747−3756. (g) Del Giacco, T.; Baciocchi, E.; Steenken, S. *J. Phys. Chem.* **1993**, *97*, 5451−5456.

Table 3. Thermochemical Properties of Oxidants and Substrates

	BDE(X–H)[a]	D(X$^+$–H$^-$)[b]	$E_{1/2}$ (V)[c]	pK_a[d]	IE (eV)[e]
$[(phen)_2Mn(O)_2Mn(phen)_2]^{3+}$			0.90		
$[(phen)_2Mn(O)(OH)Mn(phen)_2]^{3+}$	79	122	−0.01	14.6	
$[(phen)_2Mn(OH)_2Mn(phen)_2]^{3+}$	75			11.5	
$C_6H_5CH_3$[c]	90[f]	118	∼2.1	50.3	8.83
m-$C_6H_4(CH_3)_2$					8.55(2)
p-$C_6H_4(CH_3)_2$		112		53.0	8.44(5)
p-$MeOC_6H_4CH_3$		107	1.29	54.4	7.90(5)
9,10-dihydroanthracene	78[g]		∼1.5[h]		
xanthene	76[g]	90		30	7.65(2)
fluorene	74[g]				7.91(2)
naphthalene	*i*		1.55		8.14
2-methylnaphthalene					7.96(3)
1-methylnaphthalene					7.91(6)
2,6-dimethylnaphthalene					7.78(10)

[a] Bond dissociation energies, in kcal mol^{-1}. (Mn)O−H bonds from application of the thermochemical cycle in ref 44. [b] Heterolytic bond dissociation energies to remove H$^-$, from ref 28 for the organic compounds. [c] Potential for oxidation, in MeCN versus $Cp_2Fe^{+/o}$. Values for organic compounds are from ref 43. [d] In MeCN; values for organic compounds from ref 28. [e] Ionization energies; ref 50. [f] Reference 54. [g] See ref 23c for references. [h] Estimated as being the same as durene.[43] [i] The aromatic C−H bond strength in benzene is 113 kcal mol^{-1}.[50]

Scheme 4. Mechanisms for Oxidation of Alkylaromatic Compounds

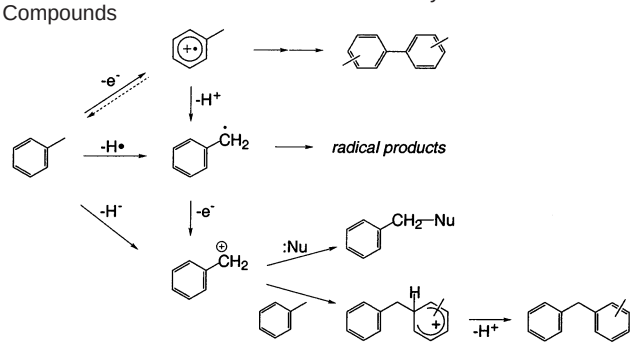

intermediacy of carbon radicals in the reactions of $\mathbf{[Mn_2(O)_2]^{3+}}$. The formation of bixanthyl and bifluorenyl implicates the presence of xanthyl and fluorenyl radicals. This is further supported by the trapping with $CBrCl_3$ to produce 9-bromofluorene, as well as the effect of added O_2 on the reactions. The primary isotope effect is consistent with initial H-atom transfer. Optical monitoring of the reactions shows that the first step is conversion of $\mathbf{[Mn_2(O)_2]^{3+}}$ to $\mathbf{[Mn_2(O)(OH)]^{3+}}$ by net addition of H$^\bullet$. $\mathbf{[Mn_2(O)(OH)]^{3+}}$ is not a result of comproportionation of $\mathbf{[Mn_2(O)_2]^{3+}}$ and $\mathbf{[Mn_2(OH)_2]^{3+}}$ because this reaction is slow. The success of the kinetic models with multiple checks supports the proposed mechanisms.

The carbon radicals are formed by a one-step hydrogen atom transfer mechanism (which could alternatively be described as a coupled proton and electron transfer). An alternative pathway of initial electron transfer and subsequent deprotonation (Scheme 4) is ruled out by the redox potentials involved. Electron transfer from DHA to $\mathbf{[Mn_2(O)_2]^{3+}}$ is uphill by ∼1.5 V or $\Delta G^\circ \cong 34$ kcal mol^{-1}, much larger than the observed $\Delta G^\ddagger$ of 21 kcal mol^{-1} for DHA oxidation. The potential for DHA is conservatively estimated as equal to that of durene (1,2,4,5-tetramethylbenzene), and following the redox potentials assembled by Eberson.[43] A mechanism of initial proton transfer is even less likely, as $\mathbf{[Mn_2(O)_2]^{3+}}$ is a very weak base and DHA a very weak acid.

The ability of a metal oxidant to abstract H$^\bullet$ is related to its thermodynamic affinity for H$^\bullet$, in other words, the strength of the bond it can make to a hydrogen atom.[3c,23,24] This bond strength is in essence the sum of the affinity for H$^+$ (the pK_a) and e$^-$ (the redox potential, *E*). The bond strengths shown in Scheme 1, 79 kcal mol^{-1} for $\mathbf{[Mn_2(O)(O-H)]^{3+}}$ and 75 kcal mol^{-1} for $\mathbf{[Mn_2(OH)(O-H)]^{3+}}$, were derived using the thermochemical cycle of Tilset and Parker[44] (following Bordwell[45]). The C−H bond strength in DHA is 78 kcal mol^{-1},[23d] so H-atom transfer to the manganese dimers is roughly thermoneutral. The bond strengths thus provide a qualitative understanding of why these reactions occur, and they are also quantitative predictors of reactivity. Rate constants for hydrogen atom abstraction from DHA (per hydrogen, at 30 °C) roughly correlate with bond strengths for abstraction by various metal complexes and oxygen radicals, as shown in Figure 7. The line drawn in this figure is defined by the values for ^{t}BuO• and ^{s}BuOO•, to show a perfect correlation. Such a Bell−Evans−Polanyi correlation is typical of hydrogen atom transfer reactions.[22] The rates of H-atom abstraction by $\mathbf{[Mn_2(O)_2]^{3+}}$ and $\mathbf{[Mn_2(O)(OH)]^{3+}}$ also correlate with the substrate C−H bond strengths (Table 1).

We have recently shown that rates of hydrogen atom transfer reactions depend on both bond strengths (driving force) and intrinsic barriers, the latter being revealed in self-exchange rates.[25] Unfortunately, hydrogen-atom self-exchange rates are not easily determined for $\mathbf{[Mn_2(O)_2]^{3+}}$/$\mathbf{[Mn_2(O)(OH)]^{3+}}$ or for $\mathbf{[Mn_2(O)(OH)]^{3+}}$/$\mathbf{[Mn_2(OH)_2]^{3+}}$, all being NMR silent. The Polanyi correlation in Figure 7 essentially assumes that the manganese dimers' intrinsic barriers are similar to those for the oxygen radicals and for the iron tris(biimidazoline) system we have examined.[46] The fact that the manganese dimers lie below the line in Figure 7 may reflect a larger intrinsic barrier,[8] which would be consistent with the slow comproportionation of $\mathbf{[Mn_2(O)_2]^{3+}}$and $\mathbf{[Mn_2(OH)_2]^{3+}}$.

(B) Electron Transfer to $\mathbf{[Mn_2(O)_2]^{4+}}$. The dehydrocoupling of arenes to biaryl derivatives (the Scholl reaction[47a]) occurs by an electron transfer mechanism (Scheme 4).[3b,40f,42d,48] The

(43) (a) Reference 3a, p 44, based primarily on (b) Howell, J. O.; Goncalves, J. M.; Amatore, C.; Klasnic, L.; Wightman, R. M.; Kochi, J. K. *J. Am. Chem. Soc.* **1984**, *106*, 3968−3976 and ref 42f. (c) E° for durene and Cp_2Fe given in ref 3a as 2.07 and 0.53 V versus NHE in MeCN. (d) It should be noted that a range of potentials have been reported in different sources for alkylaromatic compounds, and no source gives a consistent list for all of the substrates reported here.

(44) Parker, V. D.; Handoo, K. L.; Roness, F.; Tilset, M. *J. Am. Chem. Soc.* **1991**, *113*, 7493−7498.

(45) cf. (a) Bordwell, F. G.; Gheng, J.-P.; Satish, G.-Z.; Zhang, A. V. *J. Am. Chem. Soc.* **1991**, *113*, 9790−9795. (b) Bordwell, F. G.; Liu, W.-Z. *J. Am. Chem. Soc.* **1996**, *118*, 8777−8781. (c) Parker, V. D. *J. Am. Chem. Soc.* **1992**, *114*, 7458−7462; correction, *J. Am. Chem. Soc.* **1993**, *115*, 1201.

(46) Roth, J. P.; Lovell, S.; Mayer, J. M. *J. Am. Chem. Soc.* **2000**, *122*, 5486.

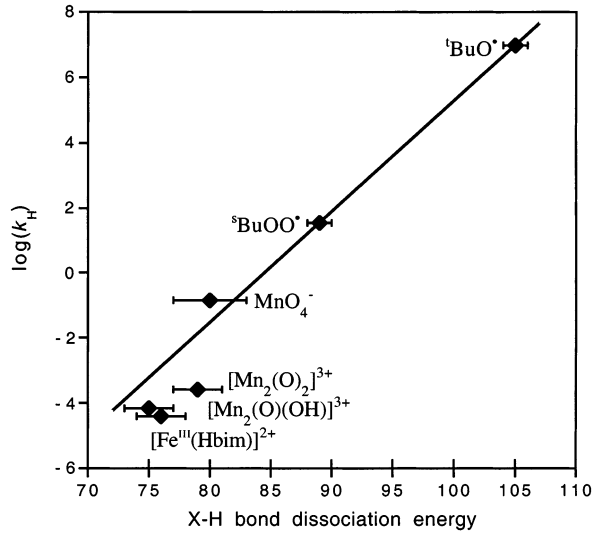

Figure 7. Plot of log k (the rate constant for hydrogen abstraction, per hydrogen) versus the strength of the X−H bond formed by the oxidants. The straight line is drawn through the two oxygen radical points.

oxidations of naphthalenes and *p*-methoxytoluene are additional examples. A mechanism of preequilibrium electron transfer is indicated by the inhibition of the oxidations of 2,6-dimethylnaphthalene and *p*-methoxytoluene by the reduced form of the oxidant, $\mathbf{[Mn_2(O)_2]^{3+}}$.[40c,42a]

Electron transfer is a reasonable pathway for $\mathbf{[Mn_2(O)_2]^{4+}}$ because this reagent, unlike $\mathbf{[Mn_2(O)_2]^{3+}}$, is a strong outersphere oxidant ($E_{1/2} = +0.90$ V vs $Cp_2Fe^{+/o}$). Electron transfer from naphthalene to $\mathbf{[Mn_2(O)_2]^{4+}}$ is uphill by only ∼0.6 V ($\Delta G° =$ 14 kcal mol^{-1}, $K_{eq} \cong 10^{-10}$). The K_{eq} indicates a maximum electron transfer rate of about 1 M^{-1} s^{-1} if the reverse reaction proceeds at 10^{10} M^{-1} s^{-1}. This is reasonably consistent with the room-temperature rate constant of 4.6 M^{-1} s^{-1} given the uncertainty in the hydrocarbon redox potentials.[43,49] The measured rates of oxidations of naphthalenes roughly parallel the relative K_{eq}'s for electron transfer, as estimated from the naphthalene ionization energies (Table 2).[50] This correlation, however, ignores changes in the rates of the step(s) that follow.

(C) Hydride Transfer to $\mathbf{[Mn_2(O)_2]^{4+}}$. The formation of substituted diarylmethanes from toluene and xylenes clearly implicates the presence of a benzylic cation which then adds to excess arene. The *N*-benzylacetamide is formed by the addition of a benzylic cation to acetonitrile solvent, followed by hydrolysis (the Ritter reaction[47b]). The large substituent effect on the rates − for example, *p*-xylene oxidized 68 times faster than toluene (a factor of 34 per methyl group) − corresponds to a Hammett ρ^+ of roughly −5. The large substituent effects are inconsistent with a hydrogen atom transfer mechanism[51] and indicate a partially cationic arene at the transition state. This could occur either by hydride or by electron transfer. Similarly, isodurene oxidation proceeding predominantly at the central methyl group (eq 6) is consistent with initial hydride or electron transfer but not hydrogen atom transfer.[52]

Electron transfer from toluene, however, is quite difficult because of its very high redox potential, 2.61 V versus NHE in MeCN (0.53 V higher than naphthalene).[43a] Electron transfer from toluene to $\mathbf{[Mn_2(O)_2]^{4+}}$ is ∼1.2 V (27 kcal mol^{-1}) endergonic, larger than the observed $\Delta G^‡ = 23.6$ kcal mol^{-1}. Given that back electron transfer cannot be faster than 10^{10} M^{-1} s^{-1}, the equilibrium constant of ∼10^{-20} means that the forward rate must be slower than 10^{-10} M^{-1} s^{-1} at 298 K. Electron transfer is therefore not kinetically competent to be a preequilibrium step in toluene oxidation by $\mathbf{[Mn_2(O)_2]^{4+}}$ with $k = 2.9$ (± 0.3) × 10^{-5} M^{-1} s^{-1} at 298 K.[53] Although there is some uncertainty associated with the redox potential for toluene, it would have to be at least 0.25 V lower to be consistent with rate-limiting electron transfer. In addition, the primary kinetic isotope effect indicates that initial electron transfer would have to be a preequilibrium, followed by rate-limiting deprotonation of the toluene radical cation. Yet toluene oxidation is not inhibited by addition of $\mathbf{[Mn_2(O)_2]^{3+}}$. The data are only consistent with a mechanism of initial hydride transfer (Scheme 1). The $\mathbf{[Mn_2(O)_2]^{3+}}$ product is apparently formed by comproportionation of $\mathbf{[Mn_2(O)_2]^{4+}}$ with the initially formed $\mathbf{[Mn_2(O)(OH)]^{3+}}$. We have been unable to determine the fate of the proton in either the oxidations or the comproportionation, because of the reactivity of $\mathbf{[Mn_2(O)_2]^{4+}}$ with bases.

III. Understanding the Choice of the Rate-Determining Step. The first step in understanding the preferred mechanism for each oxidant/substrate combination is to determine the energetics of each possible rate-limiting step. $\mathbf{[Mn_2(O)_2]^{3+}}$ and $\mathbf{[Mn_2(O)(OH)]^{3+}}$ are hydrogen atom abstracting agents because they form fairly strong bonds to H$^•$ (79 and 75 kcal mol^{-1}), a result of their high affinity for both an electron and a proton (H$^•$ ≡ H$^+$ + e$^-$). H-atom abstractions from DHA and xanthene [D(C−H) = 78, 76 kcal mol^{-1}][23d] are close to thermoneutral, while abstraction from toluene [D(C−H) = 90 kcal mol^{-1}][54] is too far uphill. $\mathbf{[Mn_2(O)_2]^{4+}}$ has a much higher redox potential than $\mathbf{[Mn_2(O)_2]^{3+}}$, but it does not act as a hydrogen atom abstractor because its reduced form ($\mathbf{[Mn_2(O)_2]^{3+}}$) has essentially no basicity.

$\mathbf{[Mn_2(O)_2]^{4+}}$ acts as an electron transfer oxidant because of its high redox potential, while the 0.91 V lower potential for $\mathbf{[Mn_2(O)_2]^{3+}}$ precludes it oxidizing hydrocarbons by electron transfer. $\mathbf{[Mn_2(O)_2]^{4+}}$ reacts by electron transfer for the lower-potential substrates, *p*-methoxytoluene and naphthalenes, but it is apparently not a potent enough outersphere oxidant to remove an electron from toluene. Instead, a hydride transfer mechanism is adopted. Parker et al. have reported that removal of H$^-$ from toluene requires 118 kcal mol^{-1},[28] which is essentially the same as the hydride affinity of $\mathbf{[Mn_2(O)_2]^{4+}}$, −122 kcal mol^{-1} (Scheme 1; these values were derived using the same thermochemical cycle in the same solvent, so they are directly

(47) March, J. *Advanced Organic Chemistry: Reactions, Mechanisms, and Structure*, 4th ed.; McGraw-Hill: New York, 1992; (a) p 539, (b) pp 879−880.
(48) Tanaka, M.; Nakashima, H.; Fujiwara, M.; Ando, H.; Souma, Y. *J. Org. Chem.* **1996**, *61*, 788−792.
(49) A reviewer has pointed out that one would normally expect $\Delta G^‡ > \Delta G°$ because of the intrinsic barrier λ, which would increase the discrepancy. Yet when $\Delta G°' = \lambda$, the Marcus equation predicts $\Delta G^‡ = \Delta G°'$ (ignoring work terms). In these highly endoergic reactions, the transition state closely resembles the products.
(50) IEs from NIST Standard Reference Database Number 69 − July 2001 Release (http://webbook.nist.gov/chemistry/) except for 2,6-dimethylnaphthalene from Frey, J. E.; Andrews, A. M.; Combs, S. D.; Edens, S. P.; Puckett, J. J.; Seagle, R. E.; Torreano, L. A. *J. Org. Chem.* **1990**, *55*, 606. (b) IEs are good indicators of relative redox potentials.[42f,43b]
(51) Howard, J. A.; Chenier, J. H. B. *J. Am. Chem. Soc.* **1973**, *95*, 3054−3055.
(52) Baciocchi, E.; Rol, C.; Mandolini, L. *J. Org. Chem.* **1977**, *42*, 3682−3686.
(53) Similar arguments in favor of hydride transfer and ruling out electron transfer can be found in Bunting, J. W. *Bioorg. Chem.* **1991**, *19*, 456−491 and references therein.
(54) Bierbaum, V.; DePuy, C.; Davico, G.; Ellison, B. *Int. J. Mass Spectrom. Ion Phys.* **1996**, *156*, 109−131.

comparable). Therefore, the proposed hydride transfer rate-limiting step for toluene oxidation has $\Delta G^\circ \cong -4$ kcal mol^{-1} (eq 8).

$$\mathbf{[Mn_2(O)_2]^{4+}} + \mathrm{PhCH_3} \rightarrow \mathbf{[Mn_2(O)(OH)]^{3+}} + \mathrm{PhCH_2}^+ \qquad \Delta G^\circ \cong -4 \text{ kcal mol}^{-1} \quad (8)$$

For $\mathbf{[Mn_2(O)_2]^{4+}}$ oxidizing toluene, there is a thermochemical bias of ~31 kcal mol^{-1} favoring hydride transfer over electron transfer. This bias is large enough for hydride transfer to be the mechanism used. *p*-Methoxytoluene, however, is oxidized by electron transfer even though hydride transfer is 24 kcal mol^{-1} easier: ΔG°(hydride transfer) $\cong -15$ kcal mol^{-1} and ΔG°(electron transfer) $\cong +9$ kcal mol^{-1}. Evidently, this 24 kcal mol^{-1} bias is not sufficient to favor hydride transfer. Electron transfer is evidently inherently more facile than hydride transfer; in other words, electron transfer has a much smaller intrinsic barrier than does hydride transfer.

IV. Radical Trapping by Manganese Dimers. The mechanisms for DHA, xanthene, and fluorene oxidation (Schemes 2, 3) involve trapping of intermediate radicals by $\mathbf{[Mn_2(O)_2]^{3+}}$ and $\mathbf{[Mn_2(O)(OH)]^{3+}}$. This trapping could occur either by electron transfer or by radical addition to a bridging oxo group. Electron transfers from xanthyl and fluorenyl radicals (Xn$^\bullet$, Fl$^\bullet$) to $\mathbf{[Mn_2(O)_2]^{3+}}$ have $\Delta G^\circ = -0.27$ and $+0.35$ V, respectively.[28] Uphill electron transfer from Fl$^\bullet$ is difficult to rationalize with the trapping rate constant of 2×10^4 M^{-1} s^{-1} at 50 °C. Most telling, Fl$^\bullet$ is 0.63 V harder to oxidize than Xn$^\bullet$, yet is trapped only 40 times slower. It is much more likely that trapping occurs by addition to a bridging oxo ligand and formation of a carbon−oxygen bond. Subsequent oxidation of the alkoxide ligand to the observed ketone (Xn═O, Fl═O) should be quite rapid. C−O bond formation must be highly exothermic, almost like a radical recombination, because formation of an O−H bond by H$^\bullet$ addition has $\Delta H^\circ \geq 75$ kcal mol^{-1}. The observation of faster trapping by $\mathbf{[Mn_2(O)_2]^{3+}}$ versus $\mathbf{[Mn_2(O)(OH)]^{3+}}$ is consistent with their H-atom affinities (although perhaps a smaller effect would have been predicted given the early transition state for these exothermic reactions).

It is interesting to compare the rates of radical trapping by the hydrogen atom abstractors shown in Figure 7. ^{t}BuO$^\bullet$ and ^{s}BuOO$^\bullet$ react with carbon radicals at essentially the diffusion limit by radical recombination, in other words, by C−O bond formation. MnO_4^- is also a diffusion-limited radical trap, for instance, reacting with $CH_3^\bullet$ at 1.05×10^9 M^{-1} s^{-1} in H_2O.[55] The permanganate reaction also likely occurs by C−O bond formation, as $CH_3^\bullet$ is not easy to oxidize. Because of the rapid trapping, MnO_4^- oxidations do not form radical dimer products such as bifluorenyl; they resemble the rebound mechanism discussed for hydroxylations by cytochrome P450.[2] In reactions of $[Fe(Hbim)(H_2bim)_2]^{2+}$, we have no evidence for trapping of Xn$^\bullet$ or Fl$^\bullet$ by the oxidant.[23e] In sum, the rates of H-atom abstraction by MnO_4^-, $\mathbf{[Mn_2(O)_2]^{3+}}$, and $[Fe(Hbim)(H_2bim)_2]^{2+}$ vary by less than 10^4 (the H-atom affinities vary by 4 kcal mol^{-1}), but the rates of radical trapping appear to vary by $\geq 10^7$. Perhaps steric effects are more important in these radical recombination-type processes than in the hydrogen atom abstractions, or perhaps terminal oxo ligands are inherently more reactive than bridging oxo ligands toward carbon radicals.

(55) Steenken, S.; Neta, P. *J. Am. Chem. Soc.* **1982**, *104*, 1244−1248.

Conclusions

This paper compares and contrasts the reactivity of three dimanganese complexes with various alkylaromatic substrates. $[(phen)_2Mn^{IV}(\mu\text{-}O)_2Mn^{III}(phen)_2](PF_6)_3$ ($\mathbf{[Mn_2(O)_2]^{3+}}$) and $[(phen)_2Mn^{III}(\mu\text{-}O)(\mu\text{-}OH)Mn^{III}(phen)_2](PF_6)_3$ ($\mathbf{[Mn_2(O)(OH)]^{3+}}$) oxidize 9,10-dihydroanthracene, xanthene, and fluorene by initial hydrogen atom abstraction. The radicals formed either transfer a second hydrogen (yielding anthracene), dimerize (to bixanthenyl, bifluorenyl), or form C−O bonds on reactions with the oxidant (to give xanthone, fluorenone). $[(phen)_2Mn^{IV}(\mu\text{-}O)_2Mn^{IV}(phen)_2](ClO_4)_4$ ($\mathbf{[Mn_2(O)_2]^{4+}}$) oxidizes naphthalenes and *para*-methoxytoluene to binaphthyl and biphenyl derivatives, by a mechanism of preequilibrium electron transfer. Oxidation of toluene by $\mathbf{[Mn_2(O)_2]^{4+}}$, however, yields predominantly *ortho*- and *para*-tolyl-phenylmethanes and appears to proceed by initial hydride transfer.

The thermodynamic ability of the manganese dimers to accept e$^-$, H$^\bullet$, or H$^-$ has been determined from redox potentials and pK_a values, using established thermocycles (Scheme 1). These values are critical to understanding what determines which pathway is followed. $\mathbf{[Mn_2(O)_2]^{3+}}$ and $\mathbf{[Mn_2(O)(OH)]^{3+}}$ react by hydrogen atom abstraction because they can form strong O−H bonds (79 and 75 kcal mol^{-1}, respectively). They are not, however, good outersphere oxidants, so electron transfer is not favorable. In contrast, $\mathbf{[Mn_2(O)_2]^{4+}}$ does not react by hydrogen atom abstraction because that requires accepting both an electron and a proton, and $\mathbf{[Mn_2(O)_2]^{3+}}$ has very low basicity. $\mathbf{[Mn_2(O)_2]^{4+}}$ can react either by electron transfer − it is a powerful one-electron oxidant − or it can accept a hydride ion (two electrons and a proton) to form the stable dimer $\mathbf{[Mn_2(O)(OH)]^{3+}}$. There is a large thermodynamic bias for $\mathbf{[Mn_2(O)_2]^{4+}}$ to accept a hydride rather than an electron from alkylaromatic compounds. For toluene, this bias is 31 kcal mol^{-1} and is large enough that the reaction proceeds by hydride transfer. However, $\mathbf{[Mn_2(O)_2]^{4+}}$ oxidizes *para*-methoxytoluene by electron transfer despite hydride transfer being 24 kcal mol^{-1} more energetically favorable. Electron transfer must be intrinsically more facile than hydride transfer in this system; it has a substantially smaller intrinsic barrier.

Experimental Section

General Methods. All manipulations were done in dry solvents under a N_2 atmosphere unless otherwise noted. Toluene, *p*-xylene, and *m*-xylene (Aldrich) were dried over Na/Ph_2CO and vacuum transferred prior to use. Dihydroanthracene (DHA, Aldrich) was recrystallized from water/ethanol, and fluorene (Aldrich) was purified by sublimation. DHA-d_{12} was synthesized from anthracene-d_{10};[56] DHA-d_4 and fluorene-d_2 were prepared by exchange using sodium dimsylate and DMSO-d_6, following ref 57, and $C_6H_5CD_3$[58] and $CH_3OC_6H_5CD_3$[40c] were prepared as noted. Toluene-d_8 (Cambridge Isotope Laboratories, Inc.) was dried over sodium and vacuum transferred prior to use. Dry electrochemical grade acetonitrile (Burdick & Jackson) was degassed and dispensed in the glovebox. $Mn(OAc)_2$ (Aldrich), 1,10-phenanthroline monohydrate (Lancaster), perchloric acid (Aldrich, 70% solution in water), and $H_2{}^{18}O$ (Cambridge Isotopes) were used as received. ^{n}Bu$_4$NPF$_6$ (98%, Aldrich) was triply recrystallized from EtOH, melted under vacuum, and dried under vacuum for 2 days. Other reagents were purchased from Aldrich and used as received. Literature procedures were used to prepare 2-

(56) Bass, K. C. *Org. Synth.* **1958**, *42*, 48−49.
(57) Bailey, R. J.; Card, P. J.; Schechter, H. *J. Am. Chem. Soc.* **1983**, *105*, 6096−6103.
(58) Johnstone, R. A. W.; Price, P. J. *Tetrahedron* **1985**, *41*, 2493−2501.

and 4-methyldiphenylmethanes, 2,4′,5-trimethyldiphenylmethane, 2,3′,6-trimethyldiphenylmethane, and 2,4,4′-trimethyldiphenylmethane.[59] Ring coupling of 4-methylanisole was achieved with $NOBF_4$,[60] and the benzylic products were prepared following ref 40a.

Infrared spectra were recorded on a PE1720 FTIR with DTGS detector. For both background and sample spectra, 32 scans were recorded at a resolution of 2 cm^{-1}. Solution IR spectra were recorded in acetonitrile, with manganese dimer concentrations of 15−20 mM, using a ZnSe cell with a 0.1 mm path length; acetonitrile peaks were removed by spectral subtraction. Kinetic experiments and optical spectra [reported as λ (nm) (ϵ, M^{-1} cm^{-1})] were done by monitoring the absorbance over the 350−820 nm range using a HP8452A diode array spectrophotometer equipped with a custom built aluminum cell block holder connected to a Peltier electronic control module (±0.1 °C) or a HP8453 diode array spectrophotometer equipped with a multicell transport and a constant-temperature bath. Fast reactions were monitored using an OLIS rapid scanning monochromator equipped with an OLIS USA stopped-flow apparatus and a constant-temperature bath. Global analysis of the kinetic data was performed with OLIS or SpecFit software (Spectrum Software Associates, NC).[36] Product analyses were done using an HP5890 series GC equipped with a SUPELCO Nukol fused silica capillary column and a FID detector. Mass spectometric analyses were performed on an HP5890/5971 GC-MS instrument using a Supelco SPB-1 capillary column. FAB mass spectra were taken on a VG 70 SEQ tandem hybrid instrument of EBqQ geometry.

$[(phen)_2Mn(\mu\text{-}O)_2Mn(phen)_2](ClO_4)_4$ ($[Mn_2(O)_2]^{4+}$). This compound was prepared from $MnCl_3(phen)\cdot H_2O$ following literature methods.[5] *Warning: Perchlorate salts are potentially explosive and should be handled with care.* UV/vis (CH_3CN): 580 (1550), 494 (3440), 410 (5050). IR (KBr pellet): 3468 (br), 3049 (w), 1629 (s), 1607 (s), 1582 (s), 1520 (s), 1427 (s), 1341 (s), 1315 (s), 1226(s), 1095 (br), 850 (vs), 718 (vs), 686 (m), 656 (m), 626 (m) cm^{-1}. The average Mn oxidation state was 3.95 (±0.05) by adding hydroquinone to $[Mn_2(O)_2]^{4+}$ in CD_3CN and monitoring by ^1H NMR, integrating the benzoquinone formed.

$[(phen)_2Mn(\mu\text{-}O)_2Mn(phen)_2](PF_6)_3$ ($[Mn_2(O)_2]^{3+}$). This compound was prepared as reported[7] except product precipitation used $NaPF_6$. The precipitate was washed with copious amount of Et_2O, redissolved in MeCN, and filtered through Celite. The solvent was then removed in vacuo to give an olive green solid (~80%). FAB-MS: 1152 [$(M - PF_6)^+$], 972 [$(M - PF_6 - Phen)^+$]. Anal. Calcd for $[Mn_2(O)_2]^{3+}\cdot 2H_2O$, $C_{48}H_{36}N_8F_{18}Mn_2O_4P_3$: C, 43.23; H, 2.70; N, 8.40. Found: C, 43.32; H, 2.37; N, 8.37. UV/vis (MeCN): 526 (580), 556 (460), 684 (554). IR (Nujol): 3416 (b), 1704 (s), 1629 (s), 1607 (s), 1583 (s), 1521 (s), 1427 (s), 839 (vs), 720 (vs), 686 (m), 659 (m), 642 (m) cm^{-1}. Average Mn oxidation state: 3.45 (3). $[Mn_2(^{18}O)_2]^{3+}$ was prepared by stirring $[Mn_2(O)_2]^{3+}$ and 10 $H_2{}^{18}O$ (70% ^{18}O) in MeCN for 30 min and evacuating to dryness. IR (ν[^{18}O]): 686 (665), 659 (642), 647 (636); all bands are broad, so the smaller shifts are not well resolved.

$[(Me_2phen)_2Mn(O)_2Mn(Me_2phen)_2](PF_6)_3$. This compound was prepared analogously to $[Mn_2(O)_2]^{3+}$, except that 4,7-dimethylphenanthroline was used, and $NaPF_6$ was added to precipitate the product (80%).[7] IR (Nujol): 692 (m) cm^{-1} (νMn_2O_2). UV/vis (MeCN): 526 (620), 556 (490), 684 (610). FAB-MS: 1264 [$(M - PF_6)^+$]. Using a 50/50 mixture of phen and 4,7-Me_2phen gives mixed ligand compounds by FAB-MS: $[Mn_2(O)_2(Me_2phen)_x(phen)_{4-x}](PF_6)_2^+$, $x = 0-4$.

$[(phen)_2Mn(\mu\text{-}O)(\mu\text{-}OH)Mn(phen)_2](PF_6)_3$ ($[Mn_2(O)(OH)]^{3+}$). Hydroquinone (5.1 mg, 0.045 mmol) was added to a solution of $[Mn_2(O)_2]^{3+}$ (120 mg, 0.09 mmol) in 20 mL of MeCN. The initial green solution turned brown immediately. The mixture was stirred at room temperature for 30 min, and 40 mL of Et_2O was slowly added to cause precipitation. The resulting brown solid was filtered, washed with a large amount of Et_2O, and dried in vacuo (~90%). Average Mn oxidation state: 3.07 (3). Anal. Calcd for $C_{48}H_{33}N_8F_{18}Mn_2O_2P_3$: C, 44.39; H, 2.56; N, 8.63. Found: C, 44.51; H, 2.63; N, 8.62. FAB-MS: 1153 [$(M - PF_6)^+$], 973 [$(M - PF_6 - phen)^+$]. IR (Nujol): 3380 (b), 1521 (s), 1457 (s), 1376 (s), 837 (s), 720 (s), 695 (m), 658 (w), 644 (w), 557 (s) cm^{-1}. UV/vis (MeCN), no distinct features; a few ϵ values are listed, 526 (930), 556 (700), 700 (300).

$[(phen)_2Mn(\mu\text{-}OH)_2Mn(phen)_2](PF_6)_3$. This compound was prepared following the procedure for $[Mn_2(O)(OH)]^{3+}$, using 1.0 equiv of hydroquinone. Average Mn oxidation state: 2.66 (3). Anal. Calcd for $C_{48}H_{34}N_8F_{18}Mn_2O_2P_3$: C, 44.36; H, 2.64; N, 8.62. Found: C, 45.58; H, 2.79; N, 8.44. FAB-MS: 1154 [$(M - PF_6)^+$], 974 [$(M - PF_6 - phen)^+$]. IR (Nujol): 3377 (b), 1519 (s), 1460 (s), 1372 (s), 838 (s), 720 (s), 642 (w), 556 (s) cm^{-1}. UV/vis (MeCN), no distinct features; a few ϵ values are listed, 526 (370), 556 (280), 700 (90).

Procedure for Reactions of $[Mn_2(O)_2]^{3+}$. $[Mn_2(O)_2]^{3+}$ (80 mg, 60 μmol) and DHA (21.6 mg, 120 μmol) in 3.0 mL of MeCN were heated at 65 °C for 11 h. An aliquot of the solution was analyzed by GC. The solvent was removed in vacuo, and the resulting solid was washed thoroughly with benzene to remove the organic products, filtered, and dried. The average Mn oxidation state was 2.37 (4). The oxidation of fluorene (20 mM) by $[Mn_2(O)_2]^{3+}$ (10 mM) in the presence of $CBrCl_3$ (1 M) was left at room temperature for 15 h, and the solution of fluorene in MeCN was run through a column of activated alumina before use.

Reaction of $[Mn_2(O)_2]^{4+}$ with DHA; Preparation of $(phen)_2Mn(OClO_3)_2$. A solution of $[Mn_2(O)_2]^{4+}$ (90.6 mg, 69 μmol), excess DHA, and MeCN was allowed to stand overnight at room temperature, during which the solution color changed from red/brown to yellow. GC/MS analysis showed anthracene (0.026 mmol), anthrone (0.009 mmol), and anthraquinone (0.018 mmol). Retention times, fragmentation patterns, and ^1H NMR spectra were consistent with authentic samples. The average oxidation of the final Mn product was 2.0 (± 0.05). The remaining solution was layered with ether to give yellow crystalline $Mn(OClO_3)_2(phen)_2$.

Reactions of $[Mn_2(O)_2]^{4+}$ with Methylbenzenes. In a typical procedure, a solution of $[Mn_2(O)_2]^{4+}$ (30.0 mg, 23 mmol), MeCN (5.0 mL), and toluene (1.0 mL, 9.4 mmol) was heated at 65 °C for 12 h, causing a color change to yellow-green. GC/MS analysis revealed the presence of *ortho*, *meta*, and *para*-tolyl-phenylmethanes (10 μmol, *o:m:p* = 42:7:40; comparing retention times and fragmentation patterns with authentic samples[39]), PhCHO (0.90 μmol), substituted benzophenones (0.16 μmol), and *N*-benzylacetamide (trace). Removal of the solvent in vacuo left a green/brown residue which was washed with ether and dried; the average Mn oxidation state was 3.52 (±0.05). *p*-Xylene gave 2,4′,5-trimethyldiphenylmethane (78%), a trace of the analogous benzophenone, and *p*-methyl *N*-benzylacetamide (19%); *m*-xylene gave 2,3′,4- and 2,3′,6-trimethyldiphenylmethanes (33% and 40%) as the major products. The average oxidation states of the final manganese products were 3.43 (*p*), 3.50 (*m*) ± 0.05; the organic products account for >95% (*p*), 80% (*o*) of the manganese oxidizing equivalents consumed. Ph_2CH_2 (0.19 g, 1.1 mmol) and $[Mn_2(O)_2]^{4+}$ (89 mg, 68 μmol) in MeCN (11.0 mL) for 16 h at 50 °C gave Ph_2CO (120 ± 20%); average Mn oxidation state in the product = 2.8 ± 0.1.

Reactions of $[Mn_2(O)_2]^{4+}$ with Naphthalenes. In a typical procedure, a solution of $[Mn_2(O)_2]^{4+}$ (32.5 mg, 25 μmol), naphthalene (20 mg, 160 μmol), and MeCN (5 mL) was stirred overnight at ambient temperature, turning olive green. GC-MS analysis showed binaphthyl as the sole organic product; the average oxidation of the final manganese containing product was 3.54 (±0.05). Reactions with methylnaphthalenes and 4-methylanisole were analogous, except that the color changes were immediate upon mixing.

Electrochemical Measurements. Cyclic voltammograms were recorded at room temperature using a BAS B-100W potentiostat under N_2 in freshly distilled dry MeCN with 0.1 M $^nBu_4NPF_6$ using Pt wire and Pt disk working and auxiliary electrodes. The reference electrode was a silver wire in 0.1 M $AgNO_3/CH_3CN$; Cp_2Fe or $(C_5Me_5)_2Fe$ was

(59) Reference 40d and (a) Tanaka, S.; Uemura, S.; Okano, M. *J. Chem. Soc., Perkin Trans. 1* **1978**, 431−434.
(60) Tanaka, M.; Nakasima, H.; Fujiwara, M.; Ando, H.; Souma, Y. *J. Org. Chem.* **1996**, *61*, 788−792.

used as an internal standard. Because of the quasi-reversible nature of the couples, the error for $E_{1/2}$ is estimated as ±50 mV. Concentrations of the compounds were in the range of 1−3 mM, and a scan rate of 100 mV/s was used unless otherwise noted. For $\mathbf{[Mn_2(O)_2]^{3+}}$, two quasi-reversible waves were observed, at −0.01 and 0.90 V versus $Cp_2Fe^{+/o}$ ($(C_5Me_5)_2Fe$ was used as the standard, and the $E_{1/2}$ values were converted as referenced to Cp_2Fe). For $\mathbf{[Mn_2(O)(OH)]^{3+}}$, one quasi-reversible wave was observed at −0.03 V versus $Cp_2Fe^{+/o}$, and, for $\mathbf{[Mn_2(OH)_2]^{3+}}$, one quasi-reversible wave was observed at −0.74 V versus $Cp_2Fe^{+/o}$ (in both cases, $(C_5Me_5)_2Fe$ as standard). Because of the quasi-reversible nature of these couples, the error in $E_{1/2}$ is estimated to be ±50 mV.

pK_a measurements were carried out using cyclic voltammetry in MeCN following the procedure in ref 34. Protonation of $\mathbf{[Mn_2(O)(OH)]^{3+}}$ was monitored in CVs of $\mathbf{[Mn_2(O)_2]^{3+}}$ by loss of the anodic current relative to the cathodic current in the $\mathbf{[Mn_2(O)_2]^{3+}} \rightarrow \mathbf{[Mn_2(O)_2]^{2+}}$ couple upon titration of an acid with appropriate pK_a into the electrochemical solution. pK_a values of the reference acids in MeCN were from ref 33. Titration using 1 equiv of NH_4PF_6 (pK_a = 16.46) had no effect on the CV, while 1 equiv of anilinium ($PhNH_3ClO_4$, pK_a = 10.56) causes complete loss of the anodic current. Using 2,4-lutidinium ($LuHClO_4$, pK_a = 14.05), we determined the pK_a of $\mathbf{[Mn_2(O)(OH)]^{3+}}$ to be 14.6 ± 0.5 from three independent measurements. The pK_a of $\mathbf{[Mn_2(OH)_2]^{3+}}$ was measured similarly by monitoring the loss of the anodic current in the $\mathbf{[Mn_2(O)(OH)]^{3+}} \rightarrow \mathbf{[Mn_2(O)(OH)]^{2+}}$ couple upon titration. Using 1 equiv of either NH_4PF_6 or $LuHClO_4$ has no obvious effect on the CV; by using $PhNH_3ClO_4$, the pK_a was determined to be 11.5 ± 0.5.

Kinetics. All kinetic runs were done under pseudo-first-order conditions; the following are typical procedures. A quartz cuvette equipped with septum screw cap (Spectrocell) containing a solution of $\mathbf{[Mn_2(O)_2]^{3+}}$ (4.0 mg, 3.0 mmol) in MeCN (2.5 mL) was equilibrated at the desired temperature in the spectrophotometer. A 1.0 mL aliquot of a solution of xanthene (18.1 mg) in MeCN (3 mL) was added to the cuvette via syringe. Accumulation of spectra was started immediately and every 180 s for 36 000 s. Three runs were done at each temperature with varying concentrations of xanthene. The stopped-flow instrument was used to collect initial data at 40 and 50 °C, with a spectrum taken every 1 s. Upon completion, solutions were analyzed by GC/MS using bifluorenyl as an internal standard (assuming the GC/MS response of bixanthenyl to be equal to that of bifluorenyl, and using independent calibration for xanthone). The reaction rates were sensitive to the purity of the solvent and the concentrations of dissolved H_2O and O_2; all of the organic substrate solutions were freshly prepared before each kinetic run, otherwise much faster rates were observed. In a similar fashion, toluene (0.25 mL, 2.35 mmol) was added by syringe to an equilibrated solution of $\mathbf{[Mn_2(O)_2]^{4+}}$ (2.0 mg, 1.5 μmol) in MeCN (3.0 mL) in the spectrophotometer. The final solutions were analyzed by GC/MS, and the kinetic data were fit at 494 or 526 nm or modeled using SpecFit with similar results. The kinetics of the methyl-naphthalene oxidations were examined by stopped-flow, monitoring the decay of $\mathbf{[Mn_2(O)_2]^{4+}}$ at 500 nm; pseudo-first-order plots were linear to 3 half-lives.

Crystallographic Studies. Crystals of $[(phen)_2Mn(\eta^1\text{-}OClO_3)_2]$ were grown by slow diffusion of ether into an acetonitrile solution and mounted on a glass fiber with epoxy. Data were collected at 161 K on an Enraf-Nonius KappaCCD diffractometer using Mo Kα radiation (λ = 0.7107 Å). The data were scaled and averaged using HKL SCALEPACK which applies a correction factor to the reflections essentially correcting for the absorption anisotropy. All heavy atoms were refined anisotropically by full matrix least-squares. Hydrogen atoms were located by difference Fourier methods and refined with a riding model.

Acknowledgment. We are grateful to the NIH (R01 GM50422-05) for financial support of this work. J.M.M. and M.A.L. also gratefully acknowledge insightful discussions with Dr. L. Eberson.

Supporting Information Available: Details of the X-ray structure of $[(phen)_2Mn(\eta^1\text{-}OClO_3)_2]$ (PDF). This material is available free of charge via the Internet at http://pubs.acs.org.

JA020204A